NATIONAL AERONAUTICS AND SPACE ADMINISTRATION

Technical Memorandum 33-600

Mariner Mars 1971 Attitude Control Subsystem Flight Performance

L. Schumacher

JET PROPULSION LABORATORY
CALIFORNIA INSTITUTE OF TECHNOLOGY
PASADENA, CALIFORNIA

March 15, 1973

NATIONAL AERONAUTICS AND SPACE ADMINISTRATION

Technical Memorandum 33-600

Mariner Mars 1971 Attitude Control Subsystem Flight Performance

L. Schumacher

JET PROPULSION LABORATORY
CALIFORNIA INSTITUTE OF TECHNOLOGY
PASADENA, CALIFORNIA

March 15, 1973

Prepared Under Contract No NAS 7-100
National Aeronautics and Space Administration

PREFACE

The work described in this report was performed by the Guidance and Control Division of the Jet Propulsion Laboratory.

PAGE MISSING FROM AVAILABLE VERSION

CONTENTS

CONTENTS (contd)

CONTENTS (contd)

FIGURES (contd)

PAGE MISSING FROM AVAILABLE VERSION

ABSTRACT

The Mariner Mars 1971 is the fifth generation in an evolutionary spacecraft design with the next design iteration (Viking) to be launched in 1975 Based on knowledge acquired from the successes and limitations of its predecessors, each succeeding generation of spacecraft has been improved and expanded in capability

This report describes the flight performance of the Mariner 71 Attitude Control Subsystem. Each phase of the mission is delineated and the attitude control subsystem performance is evaluated within the observed operational environment. Performance anomalies are introduced and discussed briefly within the context of general performance. More serious problems, such as the sun sensor interface incompatability, gas valve leaks, and scan platform dynamic coupling effects are given detailed analytical considerations.

It is concluded that the Mariner 71 attitude control subsystem flight performance was satisfactory The flight experience has increased our understanding of the attitude control process and thereby resulted in improved subsystem designs for future spacecraft.

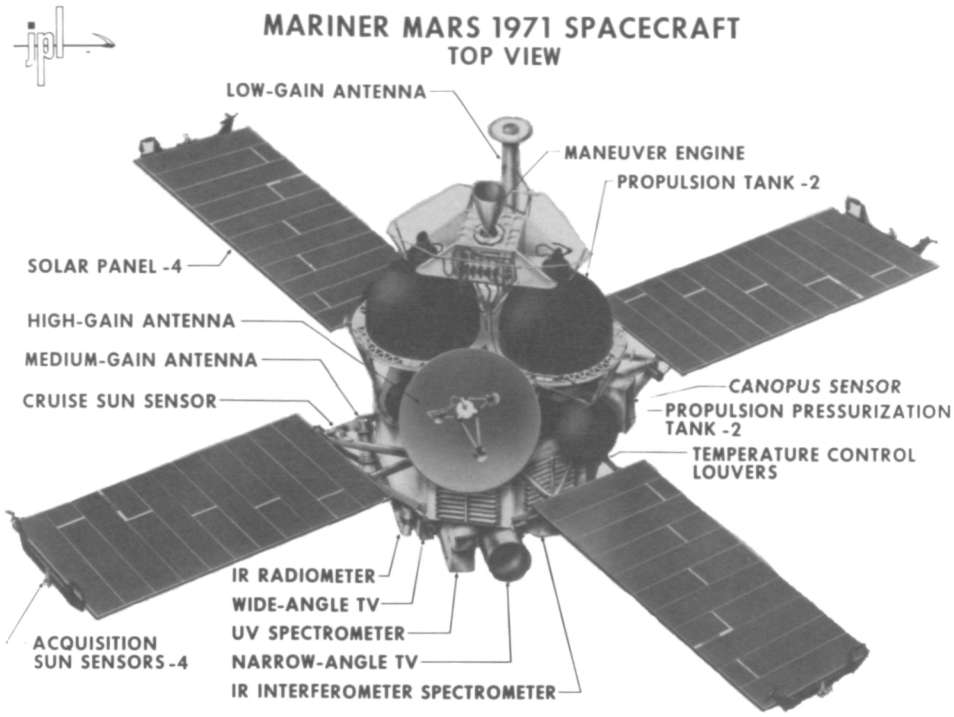

NOTE: PROPULSION MODULE AND SCAN PLATFORM INSULATION BLANKETS NOT SHOWN

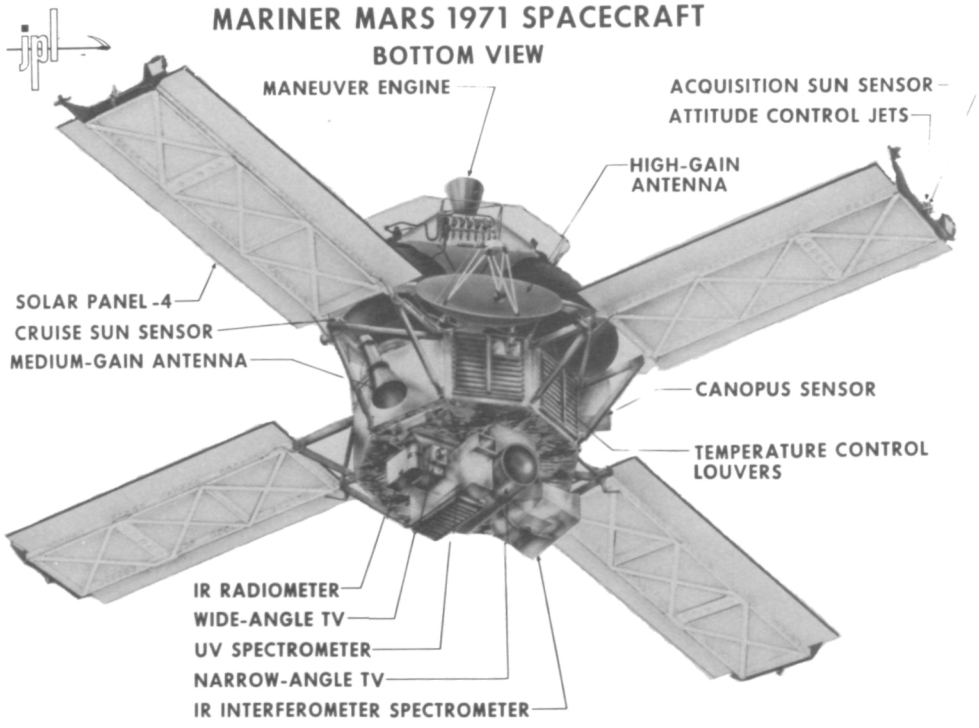

NOTE: PROPULSION MODULE AND SCAN PLATFORM INSULATION BLANKETS NOT SHOWN

I. INTRODUCTION

In its successful mission to Mars in 1971 the Mariner 71 spacecraft was the first space vehicle to orbit a planet other than Earth. The list of other scientific and engineering accomplishments of Mariner 71 is long, and all were dependent upon successful operation of the attitude control subsystem. The purpose of this report is to document the flight performance of Mariner 71 with respect to the attitude control subsystem, so that the accumulated knowledge may contribute to the success of future missions

II. ATTITUDE CONTROL SUBSYSTEM

The attitude control subsystem stabilizes and maintains flight orientation of the spacecraft from the time of its separation from the Atlas-Centaur launch vehicle throughout the duration of the mission

A SUBSYSTEM FUNCTIONS

The attitude control subsystem performs the following functions:

a Reduces the initial rates after spacecraft separation from the launch vehicle and acquires the celestial references

b Maintains correct attitude, relative to the celestial references, during transit and orbit cruise modes.

c. Performs commanded turns of the spacecraft to any desired orientation, prior to engine firing

d Controls the spacecraft orientation and the thrust vector orientation during powered flight (midcourse velocity correction, orbit insertion, and orbit trims).

e. Reacquires celestial references after powered flight and returns to the cruise mode.

f. Implements auxiliary and back-up modes.

B SUBSYSTEM COMPONENTS

The attitude control subsystem consists of celestial sensors, an inertial reference unit, a reaction control assembly, a thrust vector control system, and associated attitude control electronics

The celestial sensors include cruise and acquisition sun sensors, and a Canopus tracker

The inertial reference unit contains three single-axis, rate-integrating, strap-down gyros; a pendulous, digitally rebalanced accelerometer, and their electronics.

The reaction control assembly consists of two independent assemblies. Each assembly contains a gas storage tank, a pressure reduction valve, and six solenoid operated valves with exhaust nozzles.

The thrust vector control system includes autopilot electronics and a two-axis rocket engine gimbal actuator assembly.

The attitude control electronics contains the implementation of the control laws, and all mode selection and power switching logic

The following report will discuss the Mariner 71 attitude control subsystem flight performance. The performance of each subsystem component is evaluated as the various subsystem functions are executed

III. MISSION SEQUENCE OF EVENTS

The Mariner Mars 1971 mission can be subdivided into five discrete periods: launch, transit cruise, trajectory correction maneuvers, orbital cruise, and solar occultation. Each period has unique operational modes which, in most cases, are so dissimilar that the attitude control subsystem performance must be evaluated for each period individually.

A FLIGHT PHASES

In the flight analysis described below a general definition of each period is given, followed by the specific performance summary of the attitude control subsystem of Mariner 71. The dates and times of all significant attitude control subsystem events are summarized in Table 1.

1 The Launch Period

a. General Definition The launch period begins when the spacecraft is switched to internal power prior to liftoff (launch) and continues until gyro power is removed after acquisition of the star Canopus.

Spacecraft liftoff and ascent is the first phase of the launch period. It extends from the time attitude control power is turned on (on the launch pad) until spacecraft separation from the launch vehicle During this phase the spacecraft gyros monitor the launch vehicle angular rates during liftoff and ascent, but have no control function

Rate reduction and sun acquisition constitute the second phase of the launch period. It is an automatic sequence initiated by separation of the spacecraft from the launch vehicle A separation initiated timer admits the sun sensor and gyro error signals to the switching amplifiers, preparing the spacecraft for sun acquisition using control torques from the reaction control assembly (RCA). The spacecraft is launched into the earth's shadow without a celestial

Table 1. Mariner 71 Mission Events Related to the Attitude Control Subsystem

Event Description	Day	GMT Hr	Min	Calendar Mo/Day/Yr
Spacecraft to internal power	150	21	20	5/30/71
Lift off	150	22	23	
Spacecraft separation	150	22	36	
Attitude control on	150	22	36	
Exit earth's shadow	150	23	11	
Sun acquired	150	23	16	
Canopus acquired	151	02	25	5/31/71
Scan platform unlatch	151	23	10	
Step Canopus tracker cone angle	151	23	30	
Vent engine	152	01	28	6/01/71
Midcourse maneuver	155	22	09	6/03/71
Canopus tracker update	230	17	12	8/18/71
Sun sensor in regulation	225	00	00	8/13/71
First roll axis leak	264	20	29	9/19/71
Scan calibration No. 1	275	00	07	10/01/71
Scan calibration No. 2	281	16	00	10/08/71
Mars orbit insertion	317	16	50	11/11/71
Orbit trim No. 1	320	00	04	11/14/71
Start automatic science sequence	322	00	00	11/16/71
First Phobos interference	325	16	00	11/19/71
Roll leak clearing command action	326	00	00	11/20/71
Orbit trim No. 2	364	05	00	12/30/71
End automatic science date taking	82	00	00	3/22/72
Start engineering tests	89	17	02	3/29/72
Start solar occultation	93	00	00	4/02/72
Computer leak clearing commands initiated	136	00	00	5/15/72
End solar occultation	155	00	00	6/03/72

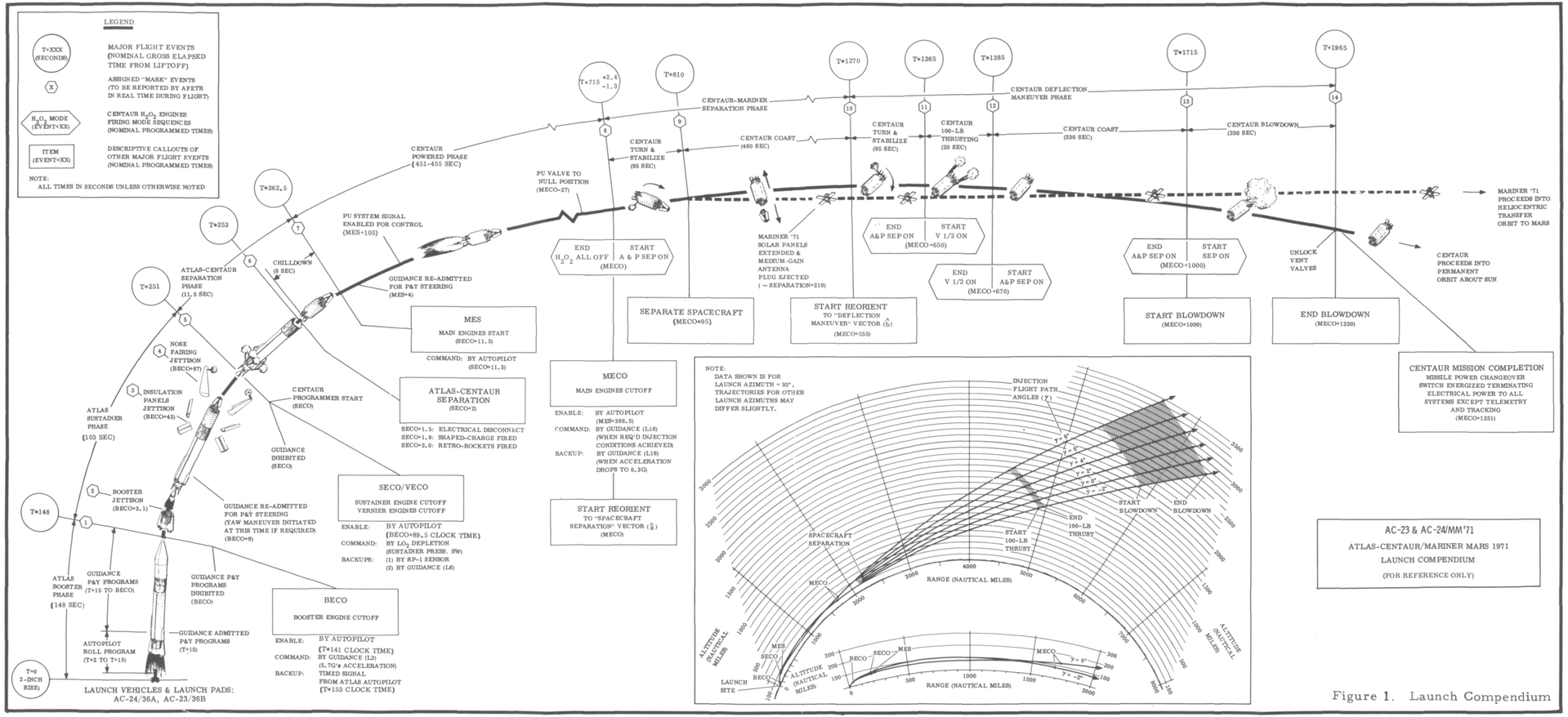

Figure 1. Launch Compendium

Page intentionally left blank

reference, and a simple rate reduction is performed Upon leaving the earth's shadow, the attitude control subsystem automatically orients the spacecraft's solar panels towards the sun Completion of celestial acquisition is delayed four hours to permit the escape of trapped gases from the spacecraft which are potentially hazardous to high voltage circuits of the Canopus tracker

Roll axis acquisition of the star Canopus is the third and last phase of the launch period. It commences with a command from the onboard control computer/sequencer subsystem, which activates the star tracker and initiates a roll axis search for the star Canopus. After acquisition of Canopus the gyros are automatically turned off, ending the launch period of the mission.

b Specific Mariner 71 Performance. The Mariner 71 launch period began when the spacecraft went to internal power at 22:08:00 on May 30, 1971 Prior to liftoff rate disturbances of about ±0 05 deg/sec, caused by wind gusts and launch vehicle propellant loading, were monitored by the attitude control gyros When the launch vehicle engines were gimballed in preflight tests, the rate disturbance exceeded 0.2 deg/sec in the pitch and yaw axes

Liftoff occurred at 22:23:04 on GMT day 150. Launch vehicle rates from liftoff to separation were observed on the spacecraft's gyro telemetry channels With each stage separation the gyros indicated large rate disturbances which were short lived as predicted The events which occurred during the liftoff sequence are illustrated in Figure 1.

The spacecraft was separated from the last stage of the launch vehicle thirteen minutes after liftoff Launch vehicle angular rates immediately before tipoff were less than 0.1 deg/sec, but after tipoff angular rates were as follows:

Pitch rate = -0.97 deg/sec
Yaw rate = -1.01 deg/sec
Roll rate = -0.27 deg/sec

These rates were reduced to within the rate deadband within 100 seconds despite the limited control torque available due to undeployed solar panels (reaction control jets mounted on panels)

The panels were deployed five minutes and eleven seconds after separation, thus providing the normal gas jet lever arm and full control torque The spacecraft left the earth's shadow thirty-five minutes and thirty-six seconds after separation The ensuing pitch and yaw axis sun acquisition appeared normal with the automatic sun-acquired signal, a "sun gate", given about four minutes after the spacecraft entered the sunlight In retrospect, however, this initial sun acquisition was the first evidence of anomalous subsystem performance

Sun acquisition performance is illustrated for either the pitch or yaw axis in Figure 2. The shaded region of the phase plane is defined as that spacecraft state where:

$$E > K_S\theta(t) + K_G\dot{\theta}(t) \tag{1}$$

The switching lines, are defined as that region of the phase plane where:

$$E = K_S\theta(t) + K_G\theta(t) \tag{2}$$

E = error signal to the switch amplifier that fires the gas jets, and is nominally = 5 μa

K_S = sun sensor scale factor, nominally $\frac{19\ 7\ \mu a}{deg}$

$\theta(t)$ = spacecraft angular position about the axis of interest

$\dot{\theta}(t)$ = spacecraft angular rate about the axis of interest

K_G = gyro scale factor, nominally $\frac{142\ \mu a}{deg/sec}$

When the sum of the spacecraft position and rate exceed the deadband, the gas jets fire to return the vehicle to within the deadband As a result, the angular rate of the spacecraft is reduced in a stepwise manner as shown in

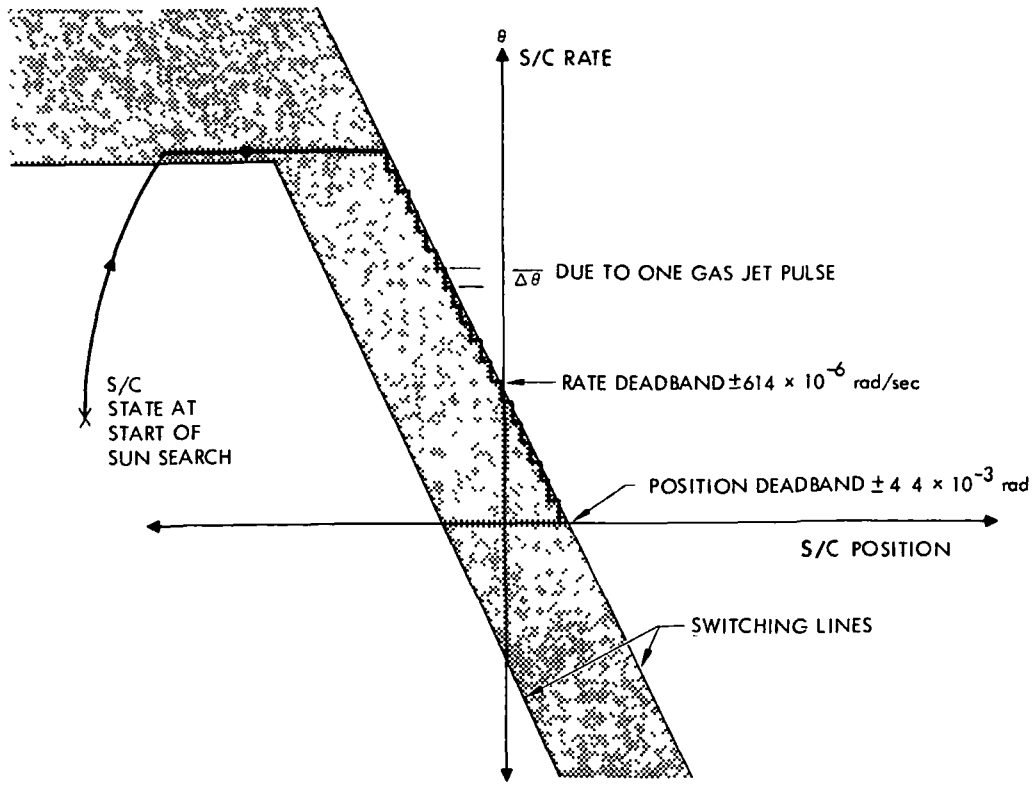

Figure 2. Phase Plane of a Sun Acquisition, in Either Pitch or Yaw Axis

Figure 2. When the total gas jet on-time is assumed to be small compared to the off-time, the time required to bring the spacecraft rate to within one gas jet pulse of zero rate is determined as follows:

$$T = \sum_{i=0} \Delta t_i \tag{3}$$

$$\Delta t_i = \frac{\Delta\theta_i}{\dot{\theta}_i}$$

$$\dot{\theta}_i = \dot{\theta}_0 - i(\Delta\dot{\theta}) \tag{3-1}$$

where

$\dot{\theta}_0$ = pitch or yaw axis sun search rate, nominally = 4 99 x 10^{-3} rad/sec

$\Delta\dot{\theta}$ = spacecraft rate increment resulting from one gas pulse
= 11 x 10^{-6} rad/sec

Δt_i = time between gas jet pulse i and (i + 1)

N = The number of gas jet pulses during time T

$$N = (\dot{\theta}_0 - \Delta\dot{\theta})/\Delta\dot{\theta}$$

$$= 454 \tag{3-2}$$

$\Delta\theta_1$ = The position displacement between each gas jet pulse.

$\Delta\theta_1$ may be evaluated from equation (2) as follows:

$$E(t) = K_S\theta(t) + K_G\dot{\theta}(t) \tag{4}$$

$$E(t + i) = K_S\theta(t + i) + K_G\left[\theta(t) - \Delta\dot{\theta}\right] \tag{5}$$

but E = E(t) at the switching time; consequently, equation (4) minus equation (5) becomes

$$\Delta\theta_1 = \frac{-K_G}{K_S}\Delta\dot{\theta} \text{ a constant}$$

Equation (3) can now be evaluated as follows:

$$T = \frac{K_G}{K_S}\frac{\dot{}}{\Delta\dot{\theta}}\left[\dot{\theta}_0 + \frac{1}{\dot{\theta}_0 - \Delta\dot{\theta}} + \frac{1}{\dot{\theta}_0 - 2\Delta\dot{\theta}} + \cdots \frac{1}{\theta_0 - N\Delta\dot{\theta}}\right]$$

$$T = \frac{K_G}{K_S}\frac{\Delta\dot{\theta}}{\Delta\dot{\theta}}\left[1 + \frac{1}{2} + \frac{1}{3} + \cdots \frac{1}{(N + 1)}\right] \tag{6}$$

$$T = \frac{K_G}{K_S}\left[1 + \frac{1}{2} + \frac{1}{3} + \cdots \frac{1}{N+1}\right]$$

$$= \frac{142}{19.7} \times 6.1 = 44.1 \qquad (7)$$

The spacecraft nominal sun search rate was to be 4 99 x 10^{-3} rad/sec and one gas jet pulse should have caused the rate to change 11 x 10^{-6} rad/sec, so that 454 total gas jet pulses should have brought the sun search rate to about zero while acquiring Using the nominal values of K_G and K_S, the time for a rate reduction should not have exceeded 44 seconds as determined from equation (7). However, the actual pitch and yaw gyro rate reduction (Figure 3) indicated that more than 50 seconds were required to reduce the yaw rate, and 109 seconds were required to reduce the pitch rate The discrepancy between predicted and actual rate reduction times, and the apparent excess gas comsumption during the launch period, resulted from a sun sensor interface design error,

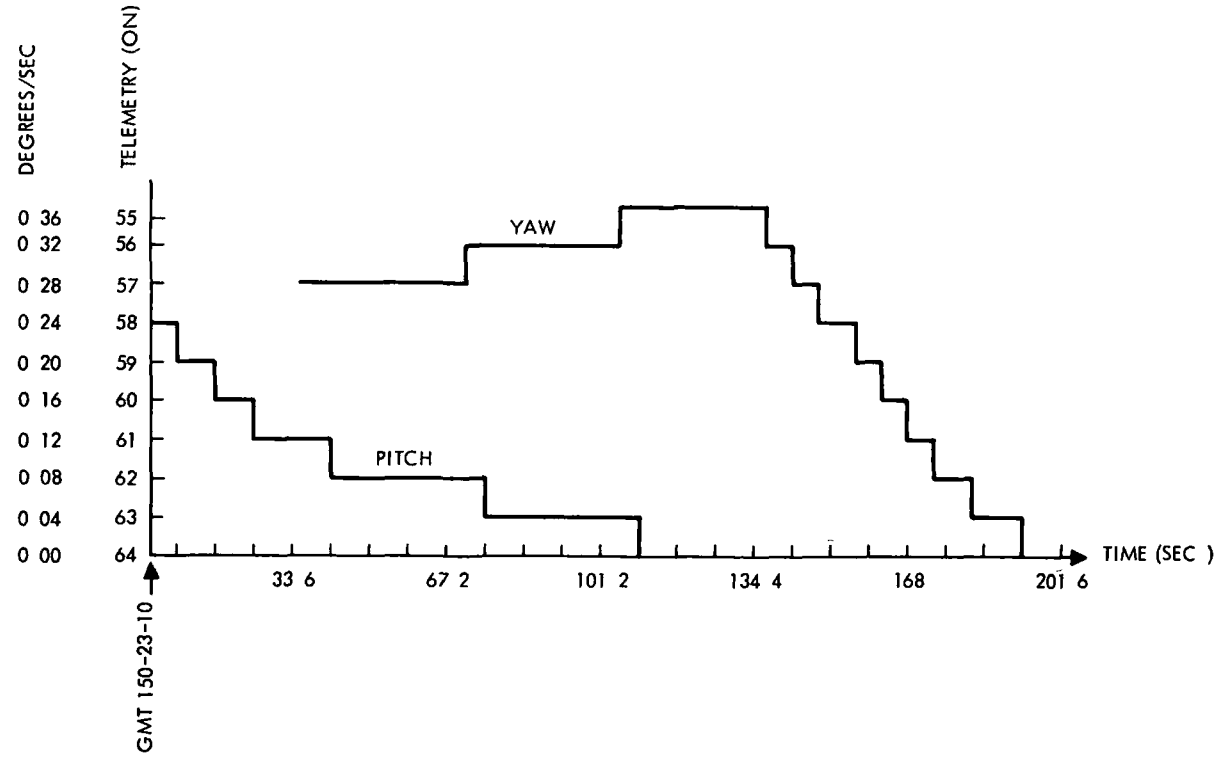

Figure 3. Pitch and Yaw Axes Angular Rate Telemetry Values During Rate Reduction

which caused the sun sensor scale factor, K_S, to be lower than normal. The interface error description, and its impact on the attitude control subsystem, is found at the beginning of Section IV

The last phase of the launch period began with a computer command activating the star tracker and initiating a search about the roll axis for Canopus. The tracker sweeps a 10-degree arc of the celestial sphere during a star search (Figure 4) and acquires all objects whose light intensity is between 0.7 and 3 5 times the intensity of Canopus

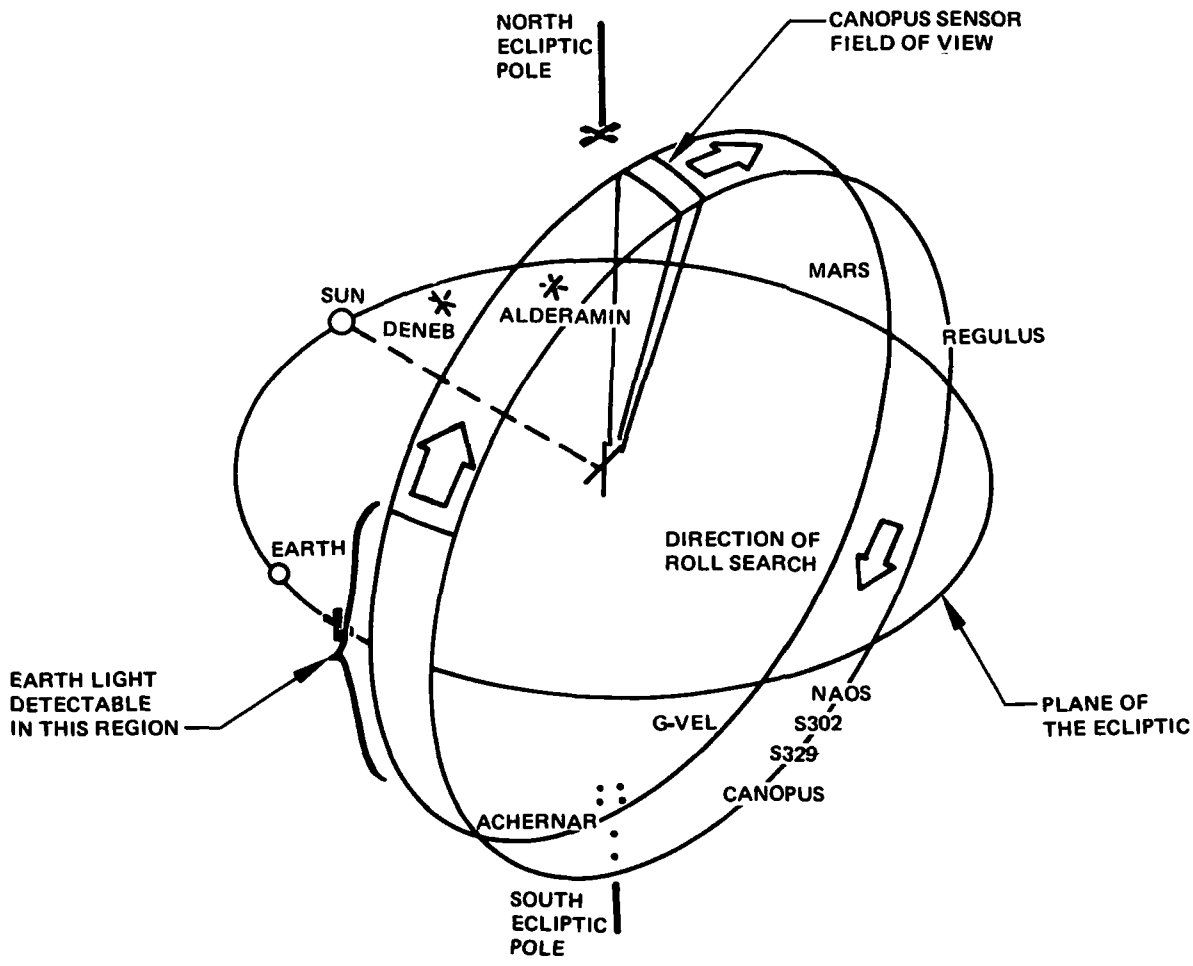

Figure 4. Roll Search Pattern

As predicted, the star Achernar, whose intensity is 0.72 times Canopus, was acquired before Canopus. The gyros were automatically shut off because the celestial acquisition criteria were satisfied A ground command was then transmitted to the spacecraft, causing the star tracker to reject Achernar and to proceed with the search for Canopus. Upon receipt of the command, the roll gyro was activated and the roll search continued, ending in acquisition of Canopus as expected

2 The Transit Cruise Period

a General Definition Transit cruise is the period of interplanetary passage between earth and Mars The transit cruise period begins when the gyros are turned off following a complete and correct celestial acquisition, and ends with the start of the Mars orbit insertion maneuver. During this period trajectory correction maneuvers are performed, instruments are calibrated, and a limited amount of scientific data is obtained.

b Specific Mariner 71 Performance The transit cruise period was initiated with a series of operations intended to transform the spacecraft from the launch state to the normal cruise state

The scientific instrument platform, or scan platform, was unlatched; the star tracker was repositioned to center the star Canopus within its field of view and the midcourse engine was vented These operations were executed on schedule and without unpredicted occurrences

By the end of day 1 of the transit cruise period, the spacecraft was oriented relative to the celestial references and all sources of disturbance from equipment outgassing and possible pressurized latching mechanism leakage had disappeared as expected and confirmed by the three celestial position telemetry signals. In spite of the apparently normal operation of the subsystem, the attitude control gas consumption was higher than anticipated.

The attitude control gas consumption can be evaluated from the sun sensor position error signal in each axis by determining the change in the angular rate of the spacecraft when the gas jets fire For example, Figure 5 illustrates a sun sensor position error telemetry signal received on earth. At point 1 the spacecraft axis has reached the maximum allowable pointing error and the gas jets are activated, causing the spacecraft to change the polarity of its angular rate in that axis The change in spacecraft rate resulting from the gas jet firings can be evaluated from the change in slope of the position error signals at the deadband edge The amount of gas used is directly proportional to that rate increment In Figure 5, the spacecraft rate as the spacecraft approaches the deadband edge is determined by the slope of the incoming line If the deadband width is known, the rate can be evaluated as follows:

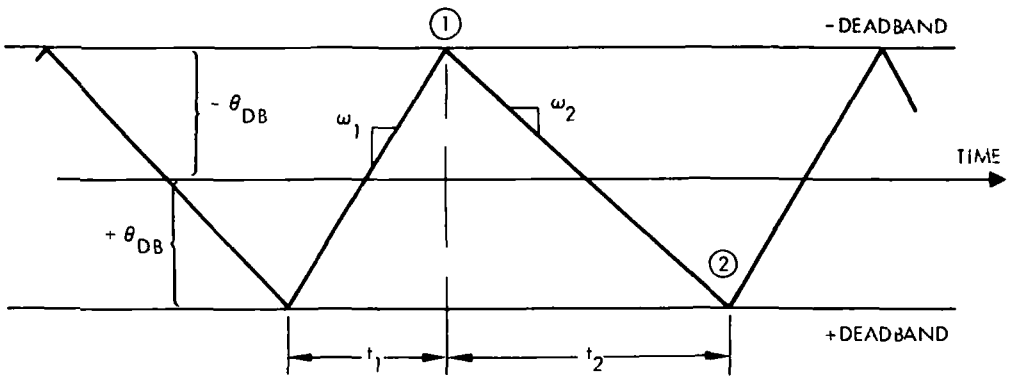

$$\Delta\theta = 2\theta_{DB}$$

$$\omega = |\omega_1| + |\omega_2| = \Delta\theta \left\{\frac{1}{t_1} + \frac{1}{t_2}\right\}$$

Figure 5. Evaluation of Limit Cycle Rate Increment Caused by a Gas Pulse

$$w_1 = \frac{2\theta_{DB}}{t_1}$$

where

w_1 = spacecraft rate coming into the deadband edge at point 1

θ_{DB} = one-half the deadband width. The celestial deadbands are nominally ±0.25 deg

t_1 = time from the last gas jet firing

The spacecraft rate after the gas jet firing is indicated by the slope of the line leaving the deadband edge and is evaluated in the same way as above. The total rate increment is the sum of the in and out going rate increments, and can be expressed as follows:

$$w_1 = 2\theta_{DB}\left[\frac{1}{t_1} + \frac{1}{t_2}\right] \tag{8}$$

where

w_1 = total change in spacecraft rate due to a gas jet firing at point 1 in Figure 5

t_2 = time between the gas jet firings at point 1 and point 2 in Figure 5

The total gas used during this rate change is:

$$W_T = \frac{Iw_1}{I_{sp}L} \text{ lb} \tag{9}$$

where

W_T = weight of N_2 consumed

I = spacecraft inertia in the axis in question

I_{sp} = specific impulse of the nitrogen gas

L = lever arm of the gas jets

Prior to launch, the anticipated rate increment in the pitch and yaw axis was 11×10^{-6} rad/sec.

It was assumed (incorrectly, as was discovered later) that the sun sensor position deadband was the nominal ±0.25 deg; thus, the observed rate increment in both axes was determined to be about 33×10^{-6} rad/sec Consequently, the gas consumption should have been approximately $0\ 77 \times 10^{-3}$ kg/day ($1\ 7 \times 10^{-3}$ lbs/day) in the pitch and yaw axes, and 1.1×10^{-3} kg ($2\ 5 \times 10^{-3}$ lbs) in the roll axis, for a total of $2\ 7 \times 10^{-3}$ kg/day ($6\ 1 \times 10^{-3}$ lbs/day).

The actual rate of gas consumption was about $5\ 4 \times 10^{-3}$ kg/day (12×10^{-3} lbs/day), as indicated by the rate of pressure change in the attitude control Reaction Control Assembly nitrogen storage bottles. The marked discrepancy between the observed gas consumption based on the assumed sun sensor deadband size and the actual gas consumption led to the discovery of a Mariner 71 sun sensor interface design error

Upon examination of the attitude control circuitry it was discovered that the zener diode regulated ±12.4 volt supply for the acquisition and primary sun sensors was incorrectly designed. The resistors returned to the ±26 volt supply are too large to provide enough current for both the sun sensors and the zener regulator (Figure 6). Therefore, the sun sensor voltage is both low and unregulated. The fact that the sun sensor voltage is low accounts for the low scale factor during sun acquisition, and the fact that the sun sensor voltage is unregulated accounts for the excessive limit cycle velocity and excessive gas consumption (Ref. 1).

A detailed explanation of attitude control subsystem operation as a result of the design error is given in Section IV.

Careful analysis, simulation, and subsystem testing revealed that the zener diodes began to conduct current and permit normal attitude control operation when the composite sun sensor bridge resistance reached about 3200 ohms

Resistance of the acquisition sun sensor bridge changed very little during the transit cruise period, but resistance of each cruise detector increased

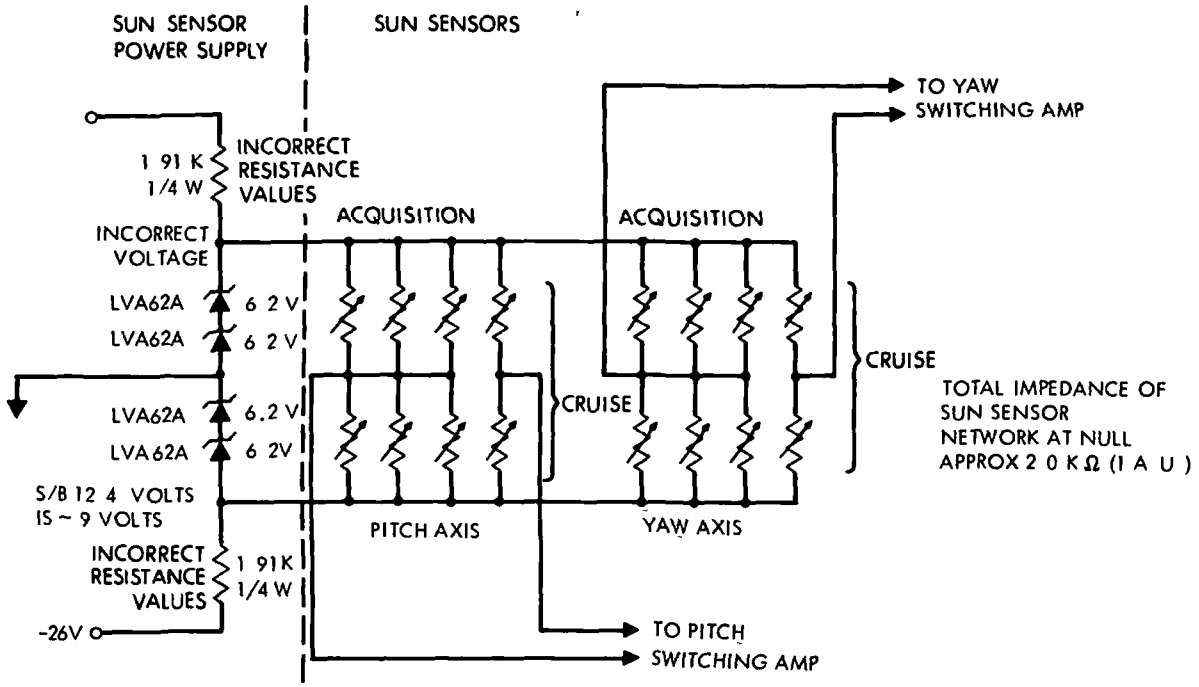

Figure 6. Incompatibly Designed Circuitry for ±12.4v Sun Sensor Power Supply

The increased resistance was caused by diminishing light intensity as the spacecraft proceeded further from the sun, and again by "detector aging." Light intensity as a function of the radial distance from the sun was known, and laboratory tests gave some indication of the detector material aging character, but the sum of both of these effects appeared to predict that the cruise sensor would never reach the necessary resistance level. However, detailed analysis of the apparent change in the rate increments at the deadband edge (see equation 8) indicated the cruise sensor resistance was increasing much faster than anticipated. Seventy-five days after launch the sun sensor circuit commenced normal operation and daily gas consumption was reduced to approximately 1.8×10^{-3} kg (4×10^{-3} lbs)

Following full regulation of the sun sensor power supply (completed on GMT day 222), the attitude control subsystem performed normally for 42 days. Then on GMT day 264, the Mariner 71 roll axis experienced a sudden positive disturbance torque of about 350 dyne centimeters. The characteristics of this anomaly indicate it was caused by a leaking roll axis RCA valve. The valve

ceased to leak and resumed normal operation in about six hours. Similar disturbance torques were observed on days 267 and 276 Beginning on day 298, they occurred almost daily During this period scan calibration exercises and limited scientific scan platform slewing were being performed, which would periodically disturb the roll axis, actuate the leaking valve, and would normally clear any existing leaks which had not cleared themselves. Most valve leaks cleared themselves after the valve was actuated for some reason.

Subsequently it was demonstrated that ground commands which actuated the leaking roll axis valve cleared most leaks The ground command enabled the roll axis gyro power which induced a transient in all the switching amplifiers and caused all spacecraft valves to fire momentarily Another gyro transient, induced when the roll gyro power was removed, also activated the leaking valve, which tended to flush out contaminants and clear the leak

The transit cruise period ended as it had started, with an attitude control subsystem problem which was causing excessive consumption of nitrogen gas

3 Trajectory Correction Maneuvers

a General Definition. A trajectory correction is a change in a spacecraft's speed and direction To accomplish the trajectory correction maneuvers, a bipropellant rocket engine aboard the spacecraft is aligned in a predetermined direction and fired until the desired velocity change is achieved The attitude control subsystem is charged with (1) precise alignment of the thrust axis of the rocket engine in the correct direction prior to engine ignition, (2) maintenance of the spacecraft attitude stability and thrust direction accuracy during the burn, and (3) reorientation of the spacecraft to the celestial references after the completion of the maneuver.

There are three types of trajectory correction maneuvers:

(1) Midcourse Maneuvers These trajectory corrections are performed during the transit cruise phase. Mariner 71 required only one midcourse correction.

(2) The Orbit Insertion Maneuver This is the longest and most critical trajectory correction During this maneuver the spacecraft velocity is reduced sufficiently to permit the vehicle to be captured by the gravitational field of Mars.

(3) The Orbit Trim Maneuver These maneuvers are performed after orbit insertion and are required to correct or change the orbit of the spacecraft around Mars

Each trajectory correction maneuver has approximately the same sequence of events First the autopilot and gyro power are enabled and the engine nozzle is permitted to move to an extreme displacement about each of the engine gimballed axes This action verifies free movement of the engine gimbals Ten minutes later the flight computer issues a command which pre-aims the engine thrust axis so that it points through the anticipated spacecraft center of mass.

The gyros are powered for two hours prior to the command that switches the spacecraft to the gyro inertial references and initiates the commanded turns This strategy permits gyro temperatures to stabilize, and minimizes gyro drift The commanded turns are a series of precisely timed turns about the roll and yaw axes of the spacecraft When the turns are complete, the thrust axis of the rocket engine is aligned in the desired thrust direction and the engine is ignited by a computer command An accelerometer measures the change in spacecraft velocity and cuts off the engine when the desired velocity change has been achieved Immediately following engine cutoff, the commanded turns are performed in the reverse order, bringing the spacecraft back into alignment with the celestial reference directions When the last celestial reference - the star Canopus - is acquired, the autopilot and gyro power are removed, and the trajectory correction maneuver is concluded

Total spacecraft performance during a trajectory correction maneuver is measured in terms of error in the desired velocity increment imparted to the spacecraft The principal contribution to that error is made by the attitude control subsystem in the form of commanded turn errors effected while positioning the thrust vector prior to the burn, and by autopilot errors incurred while maintaining the desired thrust direction during the burn Performance

evaluation of the attitude control subsystem during trajectory correction maneuvers is limited to evaluation of the commanded turn accuracy before the burn, and to autopilot performance during the burn

The autopilot performance can be evaluated roughly by monitoring the angular displacement of the rocket engine gimbal angles as the burn progresses and comparing the displacement to the predicted displacement.

b. Specific Mariner 71 Performance. The first trajectory correction maneuver of the Mariner 71 flight was performed at launch plus five days. The roll-yaw turns which positioned the thrust axis of the rocket engine in the desired direction were performed exactly as predicted. The rocket engine burn duration for the maneuver was 5.11 sec, resulting in a spacecraft velocity change of 6.720 m/sec. Because of the short burn duration, the gimbal angles were sampled but once, and indicated no discernible displacement. Error in the desired velocity increment was determined to be 0.008 m/sec.

Following the burn, the command turn unwinds resulted in acquisition of the celestial references without incident. Because the midcourse correction was so very accurate, no additional corrections were required before orbit insertion.

The orbit insertion maneuver was performed on November 11, 1971, 167 days after launch. This maneuver had the longest engine burn time of any trajectory correction and was by far the most critical. Nominally, the orbit insertion maneuver sequence would be executed identically to the midcourse maneuver, but because the timing of the orbit insertion engine ignition is so crucial, a modification of the maneuver sequence was instituted The modification was an attempt to prevent inadvertent loss of the roll axis reference (the star Canopus) in the five hour period prior to the commanded turn sequence The roll axis inertial command was inserted into the normal maneuver sequence by a direct ground command, and the maneuver was executed precisely as predicted

Pitch and yaw attitude changes measured by the gyros duplicated the predicted spacecraft angular displacement required to keep the thrust vector through the vehicle's center of mass as fuel was depleted The rocket engine gimbal angles (which respond to the pitch and yaw gyro error signals) registered a total angular movement during the burn of 2 75 degrees in one axis and 0 3 degree in the other

The rocket engine burn was of 923 seconds duration and resulted in a 1600.647 m/sec change in spacecraft velocity The error in velocity increment was 0 15 m/sec

Orbit trim maneuvers were performed on GMT day 320 and GMT day 364 The trim maneuver of day 320 had an engine burn of 6 2 seconds, resulting in a spacecraft velocity change of 15 26 m/sec The error in the desired velocity increment for this trim was determined to be 0 01 m/sec The trim maneuver of day 364 had an engine burn of 17 3 seconds, and a spacecraft velocity change of 41 9 m/sec, with an error of 0 115 m/sec

Preflight analysis and testing were unable to accurately predict the magnitude of the rocket engine swirl torque Therefore, it was desirable to determine, if possible, the swirl torque during an engine burn. Since the thrust axis of the rocket engine is approximately aligned with the spacecraft roll axis, the exhaust gas swirl torque was observed as a spacecraft roll axis disturbance torque

The roll axis inertial error signal during the orbit insertion burn is illustrated in Figure 7. A direct evaluation of this torque is not possible since the two parameters required to evaluate the disturbance torque (the period and amplitude of the position displacement between gas jet firings) cannot be determined in the inertial hold mode.

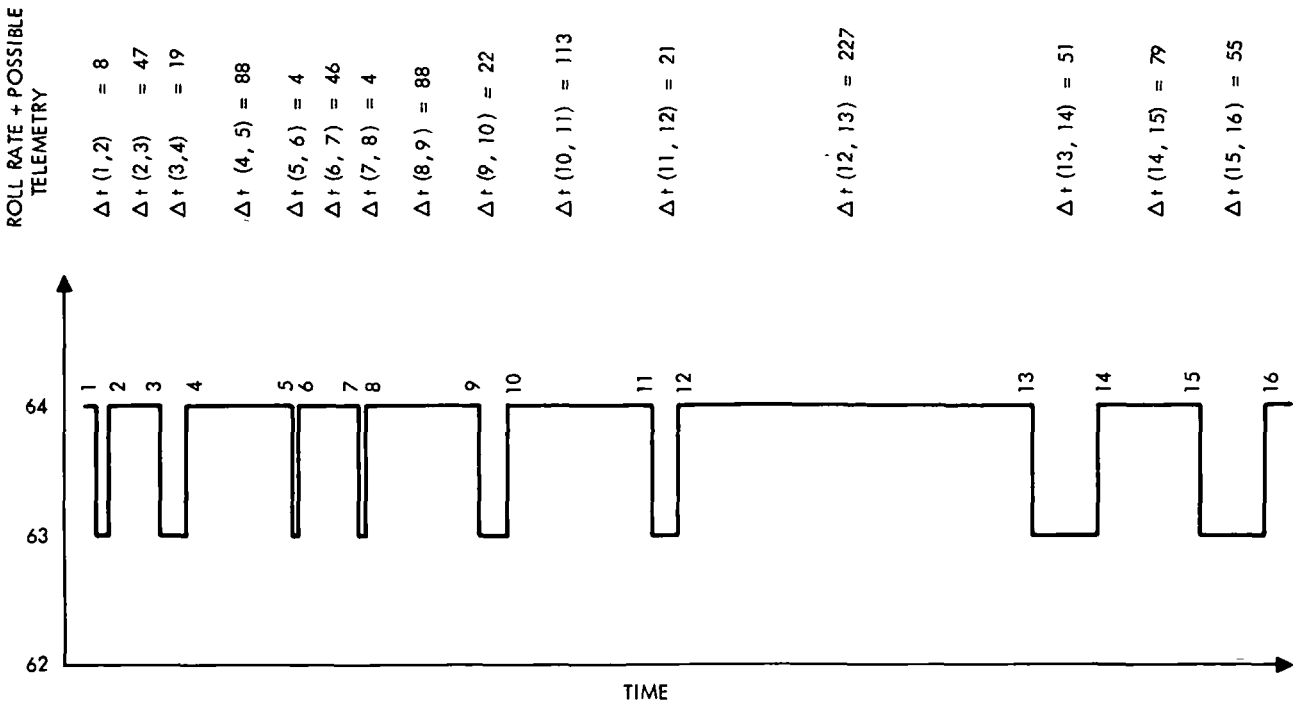

Figure 7. Roll Axis Telemetry During Mars Orbit Insertion Burn

An alternate method of torque evaluation was devised based on the following assumptions:

(1) The swirl torque is constant for the entire burn.

(2) The roll position where the telemetry values change from 63 to 64 DN and back again is fixed in the spacecraft phase plane.

A roll axis phase plane subject to a constant disturbance torque is illustrated in Figure 8. The equation of motion between crossings of the telemetry switching line is as follows:

$$\dot{\theta}(K+1) = \dot{\theta}(K) + \alpha_s \quad t(K+1, K) + N(K) \tag{10}$$

where

$\theta(K)$ = spacecraft rate at the time $t(K)$ when the telemetry switching line is crossed

$t(K+1, K)$ = time between crossings of the telemetry switching line

$N(K)$ = total gas jet rate increment in the interval $t(K+1, K)$

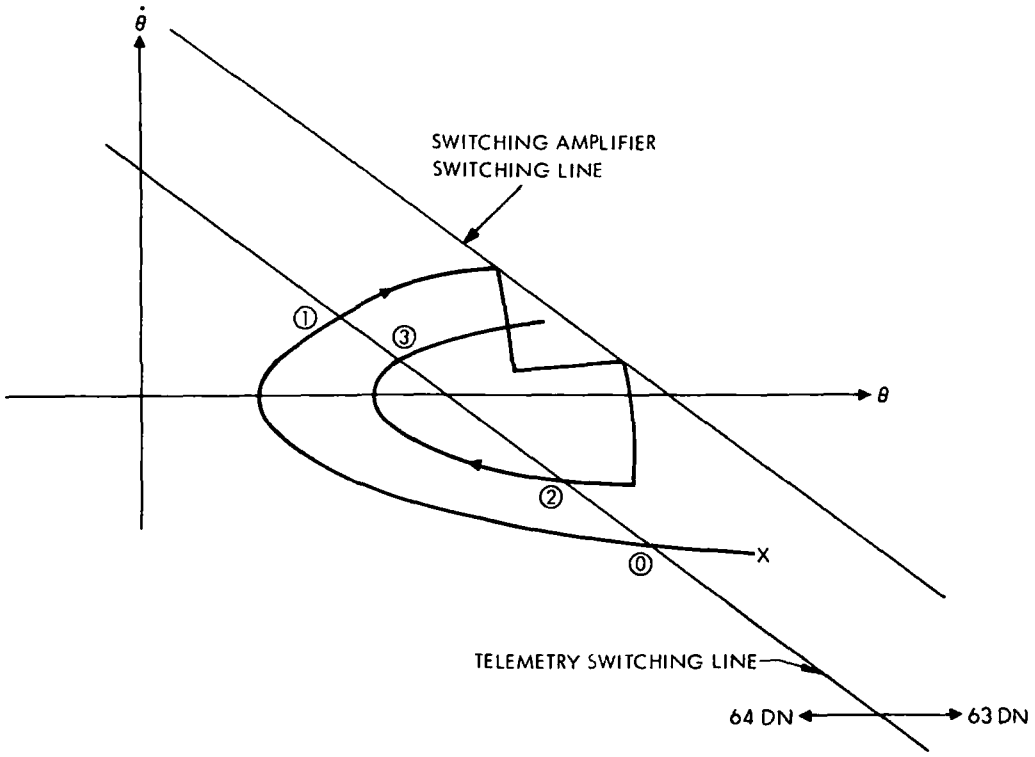

Figure 8. Roll Axis Phase Plane With Orbit Insertion Engine Swirl Torque

$$\alpha_s = \text{swirl torque acceleration}$$

$$= \text{Tor}/I(K) \qquad (11)$$

where

Tor = constant swirl torque

I(K) = spacecraft roll axis inertia in the interval t(K + 1, K)

In Figure 8, where the sum of the rate and position signal causes the telemetry value to change from 63 to 64, the following relation holds:

$$K = \theta(K) + RP \quad \dot{\theta}(K)$$

$$K = \theta(K + 1) + RP \quad \dot{\theta}(K + 1)$$

Equating the equations above reveals:

$$-RP = \frac{\theta(K+1) - \theta(K)}{\dot{\theta}(K+1) - \dot{\theta}(K)} \tag{12}$$

RP = The rate to position gain in roll inertial = 4.23 sec.

In Figure 8 it can be observed that:

$$\dot{\theta}(1) = \dot{\theta}(0) + \alpha_s t(0,1) \tag{13}$$

or

$$\dot{\theta}(0) = \dot{\theta}(1) - \alpha_s t(0,1)$$

$$\theta(1) - \theta(0) = \dot{\theta}(0)t(0,1) + \frac{\alpha_s t(0,1)^2}{2} \tag{14}$$

Substituting equation (13) into equation (14) we have:

$$\theta(1) - \theta(0) = \dot{\theta}(1)t(0,1) - \frac{\alpha_s t(0,1)^2}{2} \tag{15}$$

Also from Figure 8

$$\dot{\theta}(2) = \dot{\theta}(1) + \alpha_s t(1,2) + N(1) \tag{16}$$

and

$$\dot{\theta}(3) = \dot{\theta}(2) + \alpha_s t(2,3) \tag{17}$$

$$\theta(3) - \theta(2) = \dot{\theta}(2)t(2,3) + \frac{\alpha_s}{2} t(2,3)^2 \tag{18}$$

Replacing $\dot{\theta}(2)$ in equation (18) with equation (16) we find:

$$\theta(3) - \theta(2) = \dot{\theta}(1)t(2,3) + \alpha_s t(1,2)t(2,3) + N(1)t(2,3)$$

$$+ \frac{\alpha_s}{2} t(2,3)^2 \tag{19}$$

Substituting equations (13) and (15) into equation (12), and equations (17) and (19) into equation (12) gives:

$$-RP = \frac{\dot{\theta}(1)t(0,1) - \frac{\alpha_s}{2} t(0,1)^2}{\alpha_s t(0,1)} \tag{20}$$

$$-RP = \frac{\left[\dot{\theta}(1)t(2,3) + \alpha_s t(1,2)t(2,3) + N(1)t(2,3) + \frac{\alpha_s}{2} t(2,3)^2\right]}{\alpha_s(2,3)} \tag{21}$$

Eliminating $\dot{\theta}(1)$ from equations (20) and (21) gives

$$\alpha_s\left[t(1,2) + t\,\frac{(2,3)}{2} + \frac{(0,1)}{2}\right] = -N(1)$$

and, in general, is expressed as

$$t(K-1,K) + 2\,t(K,K+1) + t(K+1,K+2) = -2\,\frac{N(K)I(K)}{Tor} \tag{22}$$

It can be shown that

$$N(K)\ I(K) = n(K)\ W(0)\ I(0)$$

where

$W(0)$ = the gas jet induced roll rate increment at burn start
$I(0)$ = the roll inertia at burn start
$n(K)$ = the integer number of gas jet firings in the interval $t(K, K+1)$

By selecting n (K) as integer values, a consistent torque value may be found which satisfies all of the possible sequences described below:

$$Tor = \frac{-2\ n\ (K)\ W\ (o)\ I\ (o)}{t\ (K-1,\ K) + 2\ t\ (K,\ K+1) + t\ (K+1,\ K+2)} \tag{23}$$

The minimum disturbance torque which could cause the roll axis telemetry sequence during the motor burn (Figure 7) is determined to be 202 ±50 x 10^{-6} newton-meters (149 ±37 x 10^{-6} ft-lb)

The method of torque evaluation used above implies that integer multiples of the above torque could also cause the observed telemetry sequence However, because of the highly damped nature of the inertial hold mode, the minimum number of gas jet pulses must be assumed during each gas jet firing sequence or the disturbance torque must be assumed to be increasing Since the midcourse engine thrust level is approximately constant during most of the burn interval, the swirl torque also must be assumed constant, and probably has the value stated above.

4 The Orbital Cruise Period

a General Definition. Mariner 71 will remain in orbit for many years The period of principal data acquisition is the orbital cruise period. This period begins when Canopus is acquired following the orbit insertion maneuver By definition, the period ends when the planet Mars begins to occult the sun or the solar occultation period begins During the orbital cruise period, the principal activity of the spacecraft is scientific data gathering, especially TV pictures of Mars Scientific instruments, including the TV cameras, are mounted on a scan platform on the shadowed side of the spacecraft, as illustrated in the frontispiece

The scan platform is required to move from one target to another rather rapidly as the spacecraft passes close to Mars During these movements large reaction torques are experienced by the spacecraft, but the attitude control subsystem is required to hold the spacecraft rate and position within small tolerances to assure accurate targeting and minimize TV picture smear.

b. Specific Mariner 71 Performance The orbital cruise period commenced with a successful orbit insertion maneuver on GMT day 318 Normal mapping operations could not begin as planned because the Martian surface was almost totally obscured by a dust storm As the dust storm continued

unabated through more and more of the planned ninety day primary mission time the need for a mission extension became more apparent A limiting factor in planning an extended mission was the attitude control subsystem's expendable gas reserve In order to plan the extended mission, it was necessary that the cost in expendable gas of each orbital operation be known accurately Careful scrutiny of the gas consumption during the various scan slewing modes revealed several dynamic effects which were costly in expendable gas, and these effects caused certain instrument platform slewing modes to be unacceptable.

The first five twelve hour orbital periods were devoted to evaluation of orbit parameters, and to execution of the first orbit trim maneuver During these orbits many roll axis valve leaks developed. Many of the larger leaks were cleared by ground commands Nonetheless, a problem of excessive and unbalanced RCA gas consumption was developing

There are two half gas systems on Mariner 71, each containing one gas storage bottle and one valve for each polarity in each axis, or 6 valves per half gas system, as illustrated in Figure 9. When a valve in a half gas system begins to leak, a torque on the spacecraft is produced If the leakage torque is sufficiently large, it will force the spacecraft against one side of the position deadband, as illustrated in Figure 10. When this situation occurs, the torque time product produced by the leaking valve must be counteracted by the torque time product of the opposing pair of valves

The reaction control assembly gas loss caused by a leaking valve can be expressed as follows:

$$W_{LA} = W_{CA} + W_{CB} \tag{24}$$

where

W_{LA} = the weight of gas leaked from RCA tank A in some interval of time

W_{CA} = the weight of gas from tank A used to compensate for the leakage torque

W_{CB} = the weight of gas from tank B used to compensate for the leakage torque

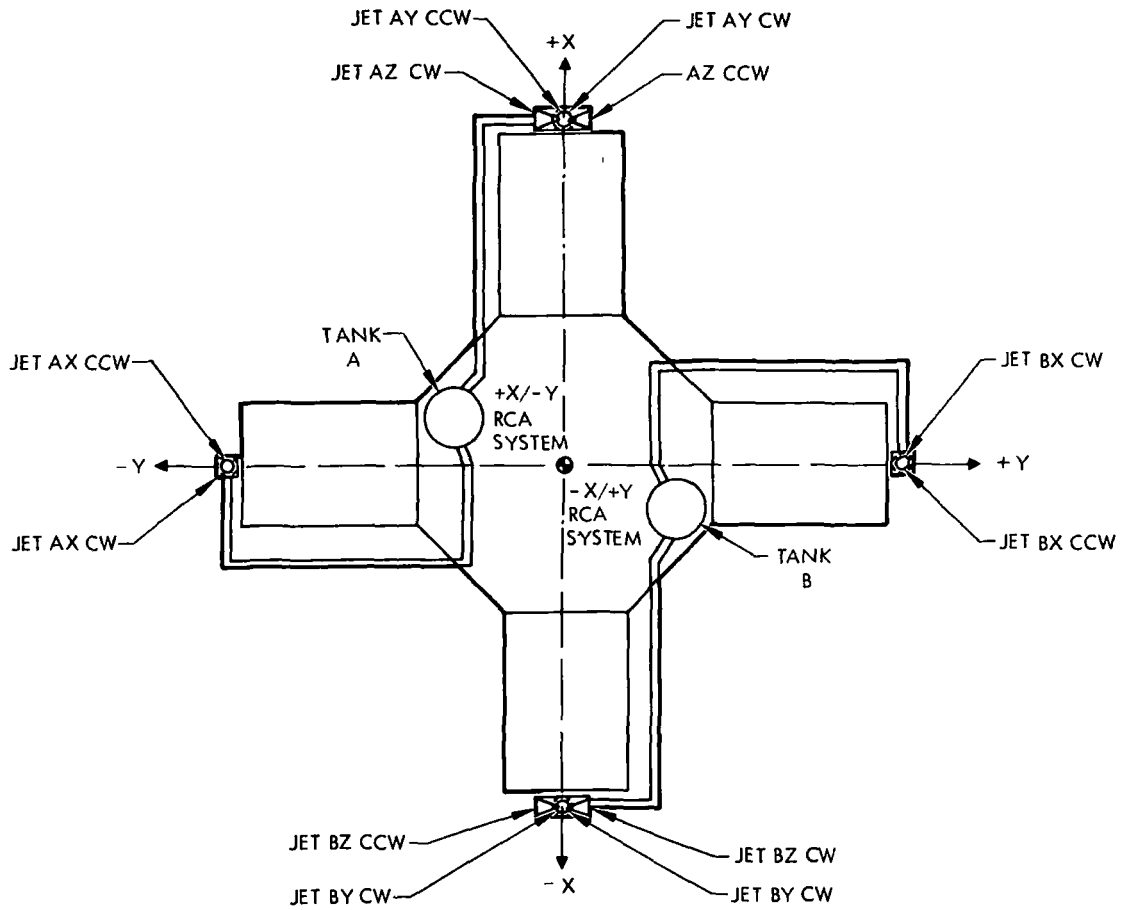

Figure 9. Reaction Control Assembly

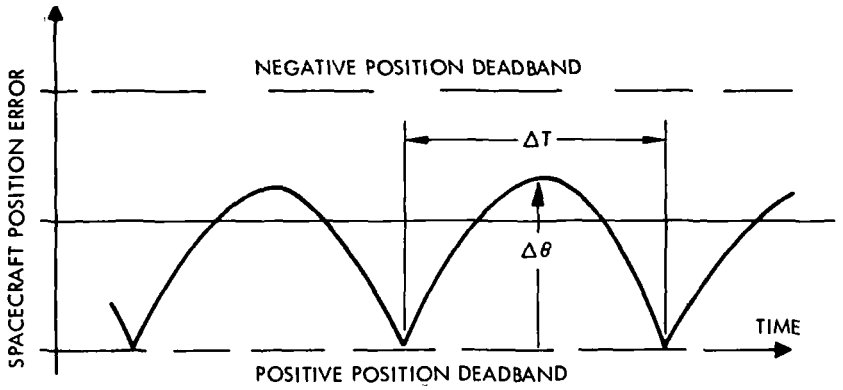

Figure 10. Spacecraft Position Error Telemetry Signal, With Positive Disturbance Torque

W_{CA} normally is equal to W_{CB}, so that

$$\frac{W_{LA}}{2} = W_{CA} = W_{CB} \quad (25)$$

The total gas consumed in both tanks because of a single leaking valve large enough to cause a one sided limit cycle is twice the total amount of gas leaked Two-thirds of the total amount of gas used due to the leak comes from the leaking tank, while one-third comes from the non-leaking tank (Ref. 2).

Prior to the development of the first roll axis leak, the -X/+Y gas storage tank (see Figure 9), contained 0.98 kg (2.16 pounds) of nitrogen, and the +X/-Y gas storage tank contained 1 kg (2 20 pounds) Following the first orbit trim maneuver three days after orbit insertion, 0.78 kg (1 72 pounds) remained in the -X/+Y tank, and 0.91 kg (2.00 pounds) remained in the +X/-Y tank Clearly, action was required to reduce the unequal rate of consumption if possible Based on the recommendation of the attitude control subsystem support team, on GMT day 326, the official mission policy was to clear roll axis valve leaks with ground commands as soon as they developed. The ground command sequence selected turned on the roll axis gyro power for one minute. This command was used because it was a reliable leak clearing sequence which had the potential to actuate the leaking valve and flush out contaminants with both the startup and shut down gyro transients. The command sequence was successful in reducing the unbalanced gas consumption from an average of $1\ 8 \times 10^{-3}$ kg (4×10^{-3} pounds) per day to about 0.45×10^{-3} kg (1×10^{-3} pounds) per day

1) Scan Platform Operation. Three days after orbit insertion, GMT day 321, scientific and TV picture taking activity commenced The scan platform, which points the science instruments, performed flawlessly. However, rate increments imparted to the spacecraft because of scan slewing were approximately fifty percent larger than anticipated.

A newly developed computer simulation technique used to study flexible bodies was employed to study the scan platform and spacecraft bus interaction (Ref. 3). The simulation duplicated the observed flight spacecraft-scan platform

interaction and implied that a significant dynamic contribution had been discovered which would make it necessary to increase the gas allotment for scan slewing by about thirty percent

2) Phobos. Eight days after orbit insertion the Canopus tracker observed a very bright object and tracked it until it left the instrument's field of view The tracker then performed a short roll search, quickly reacquired Canopus, and established the correct celestial orientation. The object which had caused the interference was the small Martian moon Phobos This interference was not anticipated by ground observers, nor could future interference periods be precisely predicted because the ephemeris of Phobos was not known accurately. To preclude losing the roll reference and many TV pictures, the spacecraft was put into the roll axis inertial mode for extended periods whenever Phobos interference was anticipated. During this period, gas consumption rose from about 5 4 x 10^{-3} kg (12 x 10^{-3} lbs) per day to 27.2 x 10^{-3} kg (60 x 10^{-3} lbs) per day.

After three or four interference periods, the orbit determination group was able to accurately predict Phobos encounters This information enabled the roll axis inertial operations to be restricted to the relatively short periods of actual Phobos interference, thereby helping to reduce the prohibitive gas consumption.

Gas consumption was indeed reduced at this time to the desired 5 4 to 6.3 x 10^{-3} kg (12 to 14 x 10^{-3} lbs) per day, but a full explanation of the spurious consumption of 40.8 x 10^{-3} kg (90 x 10^{-3} lbs) of gas was not immediately forthcoming After many computer simulations it was decided that, during the Phobos interference periods when the roll axis was in the inertial mode, dynamic interaction during scan platform slewing caused the gas jets to be fired each time the scan platform clock axis took a 0.25 degree step. Gas consumption was computed to be approximately 0.02 x 10^{-3} kg (0 045 x 10^{-3} lbs) per clock step, and about 2000 clock steps were taken in the roll inertial mode during the initial Phobos encounters

A phase plane of the spacecraft roll axis simulation during a scan clock slew is illustrated in Figure 11. The command to step the platform 0.25 degree is observed by the actuator as a step input The spacecraft reacts to

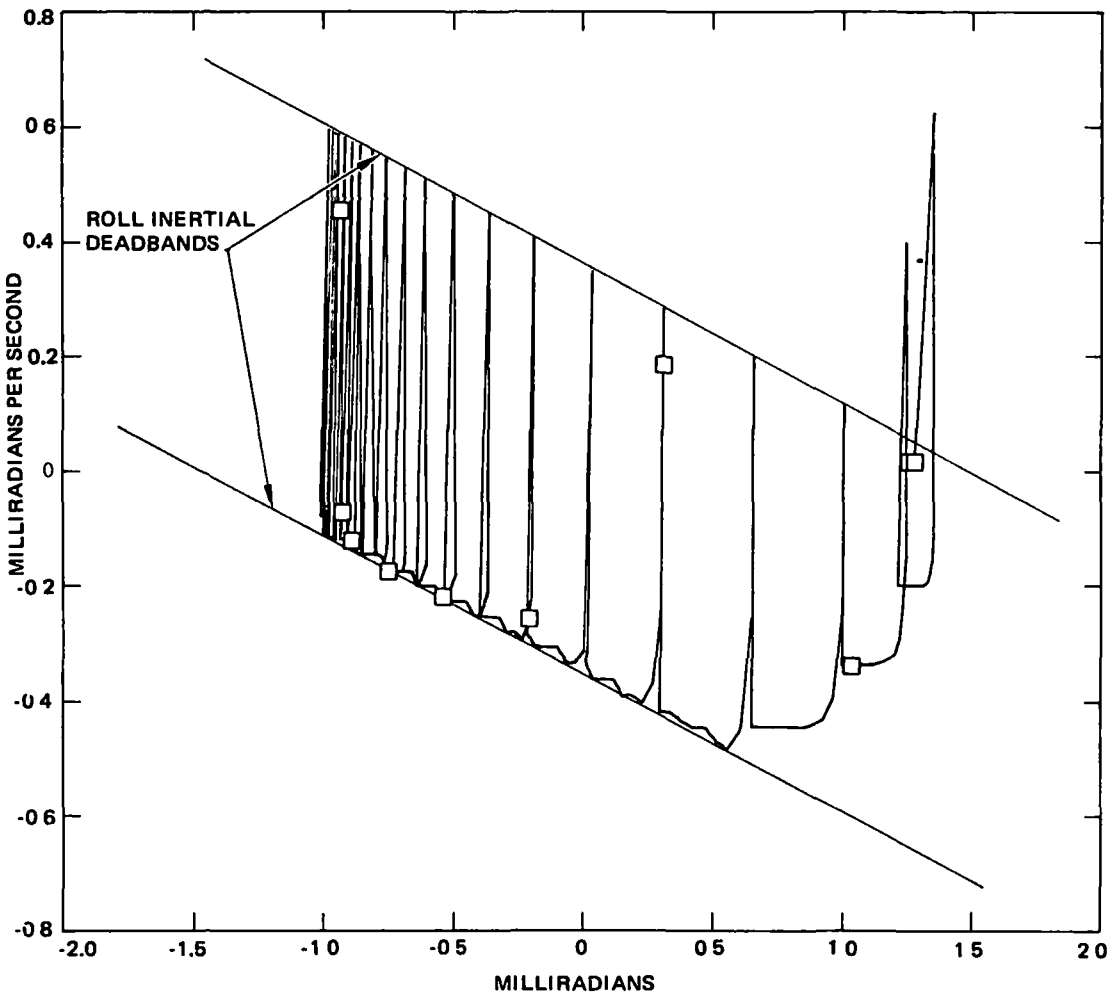

Figure 11. Roll Axis Phase Plane During a Scan Slew

the step torque input with a very large change in spacecraft rate The new rate exceeds the inertial rate plus position deadbands and fires the gas jets each time a step is taken (and sometimes afterwards) The result is an average consumption of 0.020×10^{-3} kg (0.045×10^{-3} lbs) per step, which is very close to the observed flight gas consumption. On subsequent orbits, scan slews were designed to avoid the Phobos interference periods.

3) Sun Sensor Performance In the time interval immediately following orbit insertion, it was observed that the sun sensors were periodically going out of regulation in the region of periapsis (Ref. 4).

The anomaly was caused by the total resistance of the cruise and acquisition sun sensors falling below a threshold required to keep current flowing through the zener diodes (see Figure 6). The source of the low resistance elements was not the cruise detectors, but the acquisition detectors, illuminated by reflected light from Mars

Normally, when an acquisition detector is illuminated from a point source of light, its counter part is constrained to be in the dark Consequently, the resistance of the acquisition bridge is always high. However, in the presence of a light source which may have an angular diameter in excess of ninety degrees, two or more pairs of acquisition detectors may be illuminated, such that a low resistance path exists across the power supply In the thirty minute period near periapsis where the Mars light intensity observed by the spacecraft exceeds 1614 lumen-m^2 (150 ft-candles), four to six acquisition detector resistances were reduced sufficiently to cause the sun sensor circuit to go out of regulation.

Fortunately, the operational impact of this problem was small during normal operation A restriction was imposed on the spacecraft to prevent the pitch and yaw axes gyros to be powered and in the rate mode during the out-of-regulation period There was concern that if the gas jets were to fire while the sun sensor was out of regulation, the rate feedback signal from the gyros required to turn off the gas jets would become so large that the spacecraft would be forced to keep firing back and forth until the gas supply was depleted or the sun sensor went into regulation

5) *Conclusion.* In summary, the attitude control subsystem performance during the orbital cruise period was highly satisfactory. There were operational surprises that resulted in excessive gas consumption, but the objective of precise spacecraft pointing and rate control during the science gathering orbital periods was realized In fact, not a single picture or piece of scientific data was lost during the orbital cruise period as a result of attitude control subsystem performance

5 The Solar Occultation Period

a General Description The solar occultation period begins when the spacecraft first passes through the shadow of Mars, i e , when Mars occults the sun The solar occultation period commences on orbital revolution 282 and ends on orbital revolution 406 The time in which the spacecraft is within the Martian shadow varies from a few minutes to ninety-five minutes per orbital revolution During this period of sun occultation, power for the spacecraft is supplied by batteries When the sun is in view, the batteries are recharged by solar panels

To prevent complete discharge of the batteries during sun occultation, and to insure a complete battery recharge while the spacecraft is in sunlight, all scientific instruments and unnecessary power loads must be eliminated. Since power limitations prevent the taking of scientific data, a survival mode was devised which minimizes expendable gas consumption and risk to the spacecraft An additional imposition during the solar occultation is curtailment of around-the-clock Deep Space Network tracking of the spacecraft One twelve-hour pass is allotted each working day with no coverage on weekends or during conflicts with the Apollo and Pioneer missions.

b. Specific Mariner 71 Performance The sun occultation phase of the orbital operation commenced on 1 April 1972 and continued through 5 June 1972 The major consideration during this phase of the mission was spacecraft survival, including preservation of the existing attitude control gas supply and maintenance of an adequate battery reserve.

In the planning stages of the Mariner 71 mission the possibility that the flight would extend into the solar occultation period was known, but no fixed operational plans were made. The following paragraphs briefly describe the attitude control subsystem objectives and operational restrictions which were the primary solar occultation sequence design constraints. The attitude control subsystem flight performance will be evaluated relative to the stated solar occultation performance objectives.

The principal attitude control subsystem solar occultation design objectives were:

(1) To minimize the number of cold gyro start and stop transients
(2) To prevent the occurrence of gas leaks by minimizing the number of roll axis gas jet actuations
(3) To minimize total gas consumption.

The principal operational restriction employed during the solar occultation period was limitation of spacecraft tracking to one twelve-hour pass each working day, less conflicts with Apollo or Pioneer missions The implications of this restriction are:

(1) Ground commands must be minimized
(2) The spacecraft must have the ability to automatically clear developing leaks.

The final solar occultation sequence had two operating modes. The first, and principal mode, initiated by a ground command, consisted of flight computer commands placing all spacecraft axes under inertial control during the actual occultation period. Gas consumption in this mode approximated 0.68×10^{-3} kg/orbit (1.5×10^{-3} lbs/orbit)

The secondary occultation operating mode was automatically initiated if the ground based command had not been received and the sun was occulted by Mars. In this mode the gyros were turned on when the sun was lost, but they provided only rate information, and no inertial reference was established. The spacecraft was allowed to drift at a low rate for the entire occultation period, and a reacquisition was normally required when the sun came back into view Gas consumption in the secondary mode was 4.1×10^{-3} kg/orbit (9×10^{-3} lbs/orbit).

Other features of the solar occultation sequence which were common to both the primary and secondary operational modes are:

(1) The Canopus tracker was turned off, leaving the roll axis without a celestial reference.

(2) The roll axis gyro was powered in the rate mode for the entire orbital period, except during occultation periods, when it was in the inertial mode This mode minimized roll gas leaks, total gas consumption, and gyro cold starts

(3) A Central Computer and Sequencer (CC&S) command was sent every four hours to stop any roll axis leak

The Mariner 71 solar occultation performance was exactly as predicted until GMT day 123, when the roll axis rate telemetry signal developed the signature of a roll axis valve leak The observed telemetry signature, and the probable spacecraft roll axis angular rate history producing this signature, are illustrated in Figure 12. The disturbance torque which could cause this telemetry signature may be evaluated in the following manner:

$$T_{or} = \frac{IR \times \Delta\dot{\theta}}{t} \tag{26}$$

where

T_{or} = leakage disturbance torque in ft-lbs

IR = spacecraft roll axis inertia = 470 kg-m^2 (347 slug-ft^2)

$\Delta\dot{\theta}$ = known spacecraft roll axis rate increment attributal to one gas jet pulse (30.7×10^{-6} rad/sec)

t = time between gas jet firings determined from the telemetry data (as in Figure 12)

Once the leakage torque was known, the leak magnitude could be determined in the same manner as gas leaks evaluated during orbital cruise Gas consumption in the half-gas system with the early leak history evidenced a moderate increase which agreed closely with the observed leak consumption As a result of this observation the automatic leak stopping commands were initiated on GMT day 136 about midway between occultation periods The initial results of the command action were satisfactory: the telemetry signature of a valve leak was stopped by a programmed leak stopping command (see Figure 13). However,

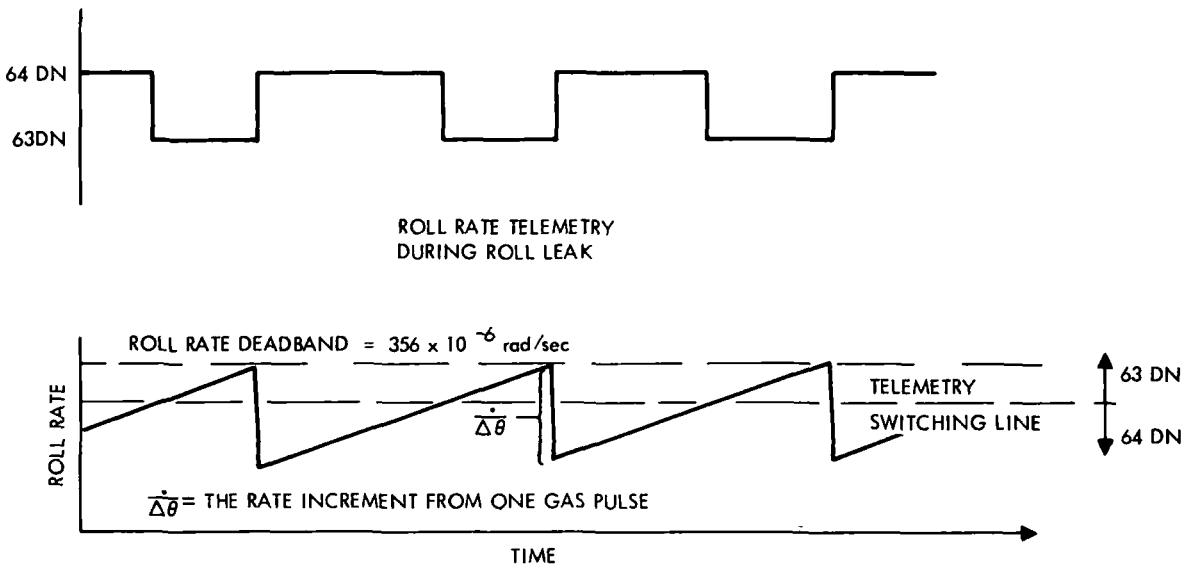

Figure 12. Roll Axis Rate History During Roll Leak

on GMT day 139 this same command appeared to have initiated a leak, indicating a failure potential in the leak stopping process. At that point the end of the solar occultation period was seventeen days away, and improvement in the leaking valve situation could be achieved only by a complete turnoff of the roll axis gyro between occultation periods However, this method was hazardous, for in the event a large leak occurred during gyro turnoff, gas would be depleted rapidly, through rate coupling into the pitch and yaw axes. It was decided therefore to attempt to reach the end of the occultation period without major sequence changes, unless the situation worsened significantly.

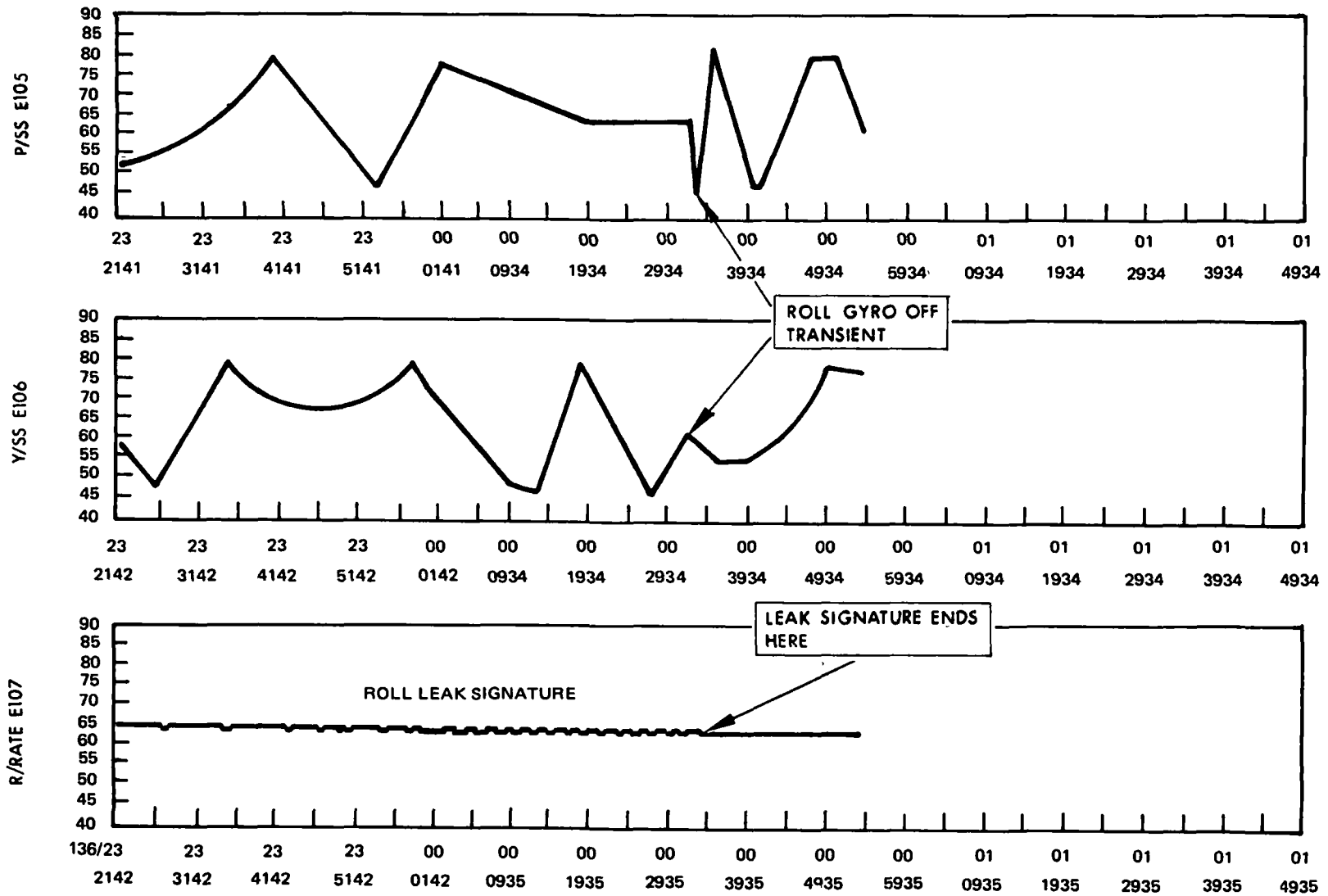

Figure 13. Three Axis Telemetry Signature of a Programmed Leak Stopping Command

IV. MARINER 71 ATTITUDE CONTROL SUBSYSTEM PROBLEM ANALYSIS

Three significant attitude control subsystem problems developed in the course of the Mariner Mars 71 mission. This section will present a short, comprehensive analysis of:

(1) Mariner 71 sun sensor interface design error.
(2) Mariner 71 RCA gas leak identification and evaluation.
(3) Mariner 71 scan platform – spacecraft dynamic interaction.

A. MARINER 71 SUN SENSOR INTERFACE DESIGN ERROR

The principal researchers and analysts involved in Mariner 71 sun sensor interface design error investigations were William E. Crawford and R. S. Edmunds. Much of the following material is extracted from their internal reports (Refs. 1 and 4).

1. The Problem

Analysis of the attitude control sun sensor circuitry revealed that the zener-diode regulated ±12.4 volt supply for the combined acquisition and cruise sun sensor bridge had been incorrectly designed. The combined cruise and acquisition sensor bridge, the zener diode voltage regulators, and the incorrectly sized current limiting resistors are illustrated in Figure 6.

2. Effects of the Unregulated Sun Sensors on the Attitude Control Switching Amplifier Circuits

With the spacecraft in the cruise operating mode, and sun sensor voltages unregulated, the firing of a valve causes a positive feedback voltage on the power supply that is returned by voltage divider action to the sun sensors This causes the amplifier to "latch up" until the derived rate can overcome the effects of the positive feedback.

In Figure 14, the composite resistance of the pitch and yaw cruise and acquisition sun sensors is assumed to be 2 0 K. This impedance causes the voltages at points C and D to be approximately nine volts Thus, the 12 4 volt zeners are not in conduction and are not regulating the voltage across the sun sensors.

Point E is the output of the pitch sun sensors as well as the input to the pitch switching amplifier When point E reaches +1.2 volts (switching amplifier deadband), the 20 millisecond minimum-on-time generator driving the clockwise valve is energized. This supplies a 20 millisecond voltage pulse to the clockwise valve H. During this 20 milliseconds the current drain through the valve loads down the negative 26 volt supply (point B), causing the voltage to go positive by 900 millivolts. Because the sun sensors form a voltage divider between the ±26 volt supplies, the positive going -26 volt supply causes a positive going voltage error at the sun sensor output. This is positive feedback and the switching amplifier will continue to energize the clockwise valve until the negative feedback path (derived rate F) produces enough voltage to overcome the input error. The clockwise valve is open 75 milliseconds, proportioned into approximately four minimum-on-time increments.

3 Sun Sensor Flight Performance

Sun sensor limit cycle data was used to observe anomalous performance of the sun sensor and to follow the recovery trend A typical limit cycle is shown in Figure 5. A change in slope of the sun sensor output occurs with each firing of a thrust valve. The rate change corresponding to a thrust valve firing can be found by comparing the slopes of the sun sensor output before and after a valve firing, provided the sun sensor scale factor is known.

The sun sensor scale factor is determined in part by the voltage applied to the sensors. Because this voltage was known to be out of regulation on Mariner 71, the scale factor could not be determined Instead, the apparent rate change, or apparent rate increment, associated with a valve firing was computed This was accomplished by setting θ_{DB} = 4 4 mrad (0.25 deg) (the designed deadband

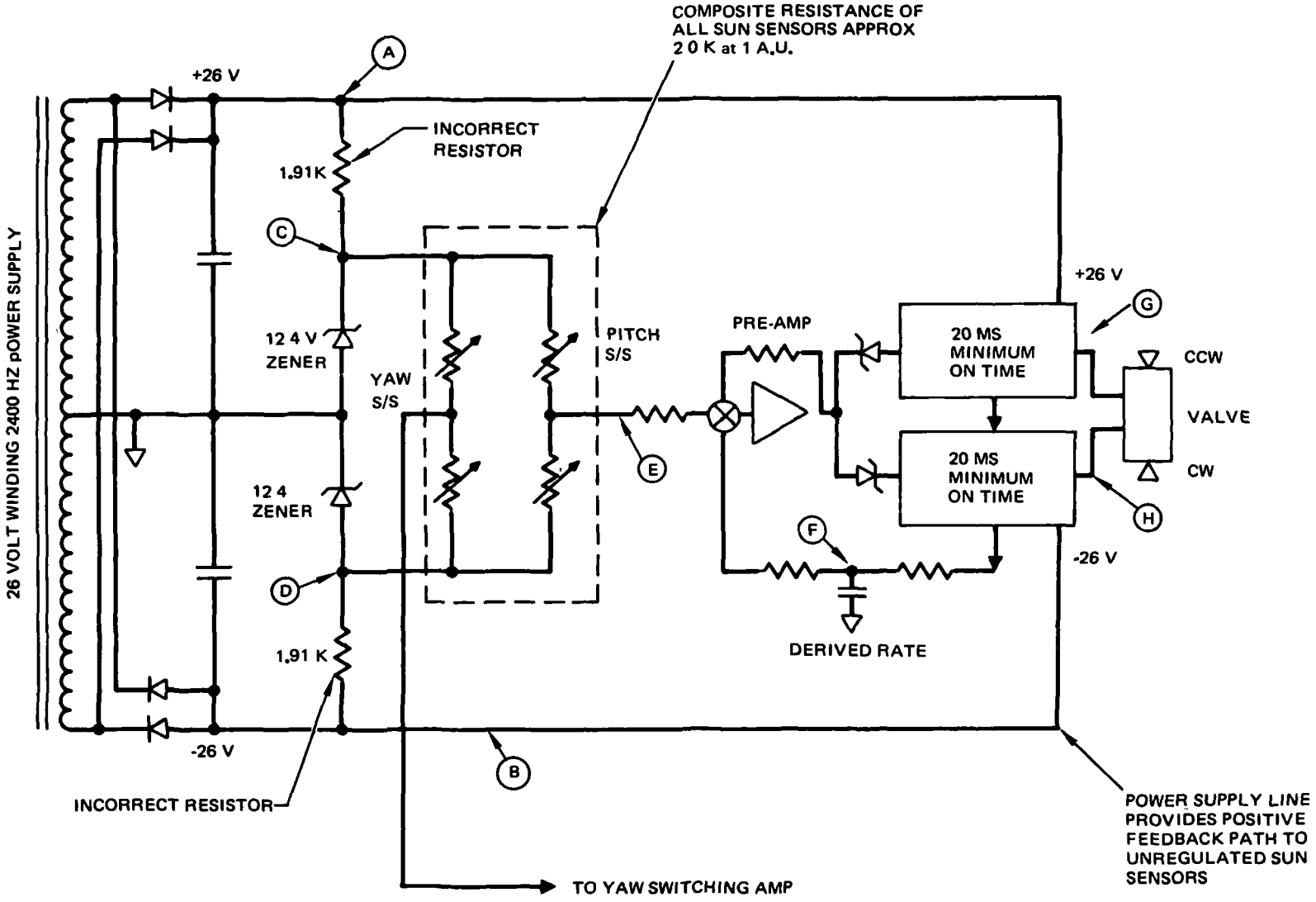

Figure 14. Sun Sensor – Switching Amplifier Circuit

size, illustrated in Figure 5), and computing Δw. The result of this computation is plotted in Figure 15.

During the initial part of the mission the apparent rate increments for the pitch and yaw axes increased, whereas the roll rates remained constant. If it is assumed that the true rate increment remained constant in pitch and yaw, as it did in roll, the increase in the apparent rate increment can be interpreted as a decrease in the deadband width. The decrease in deadband width can, in turn, be interpreted as an increase in sun sensor resistance.

Laboratory tests on the sun sensors, in conjunction with data on the flight sensors, showed that the initial sun sensor resistance was about 1.9 KΩ. The apparent rate increments described in Figure 15 provided data needed to determine the point in time that the sun sensor resistance had reached 3.2 KΩ.

4. Calculation of Deadband Width, Sun Sensor Scale Factor, and Resistance

There are two methods of calculating the deadband size. The first method requires that the launch value of sun sensor resistance be known; the second method requires that the true rate increment per value pulse be known. Both methods utilize the apparent rate increments of Figure 15.

Method 1

If the launch value of sun sensor resistance is known, the launch value of the deadband size can be calculated.

The current value of the deadband width ($\Delta\theta_2$) can then be found from the formula:

$$\Delta\theta_2 = \frac{\Delta w_1^*}{\Delta w_2^*} \Delta\theta_1 \tag{27}$$

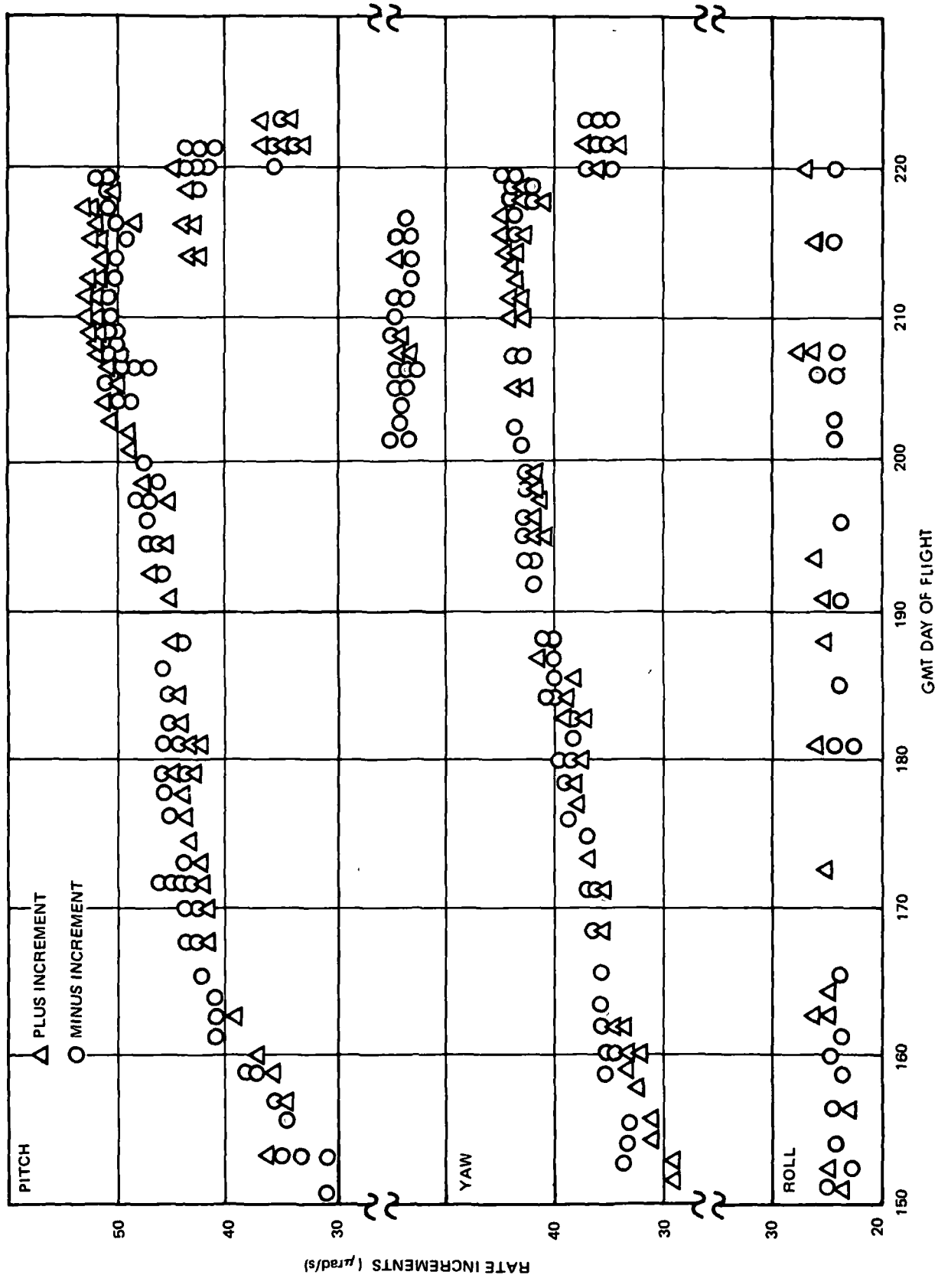

Figure 15. Apparent Limit Cycle Rate Increments

where

Δw_1^* = the apparent rate increment at launch evaluated in equation (8)

Δw_2^* = the current value for the apparent rate increment.

Equation (27) can be derived as follows:

In a typical limit cycle (Figure 5), the deadband width is not known beforehand; consequently, the nominal value $\Delta\theta^* = 8.8$ mrad (0.50 deg) is assumed. The apparent rate increment (Δw^*) is then computed from equation (8).

Let the launch value of Δw^* be given by

$$\Delta w_1^* = \frac{\Delta\theta^*}{t_1} + \frac{\Delta\theta^*}{t_2} \tag{28}$$

and the current value of Δw^* by

$$\Delta w_1^* = \frac{\Delta\theta^*}{t_3} + \frac{\Delta\theta^*}{t_4} \tag{29}$$

then

$$\frac{\Delta w_1^*}{\Delta w_2^*} = \frac{t_3 t_4}{t_1 t_2} \frac{(t_1 + t_2)}{(t_3 + t_4)} \tag{30}$$

Now the initial true rate increment is given by

$$\Delta w_1 = \frac{\Delta\theta_1}{t_1} + \frac{\Delta\theta_1}{t_2} \tag{31}$$

where

w_1 = the initial rate increment

$\Delta\theta_1$ = the initial deadband width

Similarly, the current true rate increment is given by

$$\Delta w_2 = \frac{\Delta\theta_2}{t_3} + \frac{\Delta\theta_2}{t_4} \tag{32}$$

If it is assumed that $w_1 = w_2$, equations (31) and (32) give

$$\frac{\Delta\theta_2}{\Delta\theta_1} = \frac{t_3 t_4 (t_1 + t_2)}{t_1 t_2 (t_3 + t_4)} \tag{33}$$

and comparing equations (30) and (33) we find

$$\frac{\Delta\theta_2}{\Delta\theta_1} = \frac{\Delta w_1^*}{\Delta w_2^*} \tag{34}$$

which proves equation (27), provided the true rate increment remains constant.

A plot of the roll axis rate increment is given in Figure 15. The Δw for roll is seen to be constant; therefore, Δw for pitch and yaw also may be presumed to be constant.

Method 2

The second method for determining the current value of the deadband requires that the true rate increment (Δw) be known. The current value of the deadband width is then found from

$$\Delta\theta = \frac{\Delta w}{\Delta w^*} \Delta\theta^* \tag{35}$$

Equation (35) can be derived as follows:

The true rate increment is given by

$$\Delta w = \frac{\Delta\theta}{t_1} + \frac{\Delta\theta}{t_2} \tag{36}$$

and the apparent rate increment by

$$\Delta w^* = \frac{\Delta\theta^*}{t_1} + \frac{\Delta\theta^*}{t_2} \tag{37}$$

Taking the ratio of equations (36) and (37) gives

$$\frac{\Delta w}{\Delta w^*} = \frac{\Delta\theta}{\Delta\theta^*} \tag{38}$$

This is the same as equation (35).

To use Method 2, the true rate increment is found independent of limit cycle data as described in Reference 5, and Δw^* is found as described above.

The results of the two methods of calculating deadband width are given in Figure 16. P_1 and Y_1 identify the pitch and yaw apparent rate increment estimates, using Method 1. P_2 and Y_2 identify the estimates using Method 2. It can be seen that Method 1 estimates are slightly higher than those for Method 2, but they agree within about 10 percent.

As part of the above investigation, it was determined that the rate increments imparted to the spacecraft by one RCA gas jet pulse was over fifty percent greater than values estimated prior to launch. In addition, the cruise sun sensor regulated pitch and yaw position deadband size just prior to regulation was found to be between 3.66 and 4 0 mrad (0.21 and 0.23 deg), which is between 8 and 16 percent below the design width of 4 4 mrad (0 25 deg)

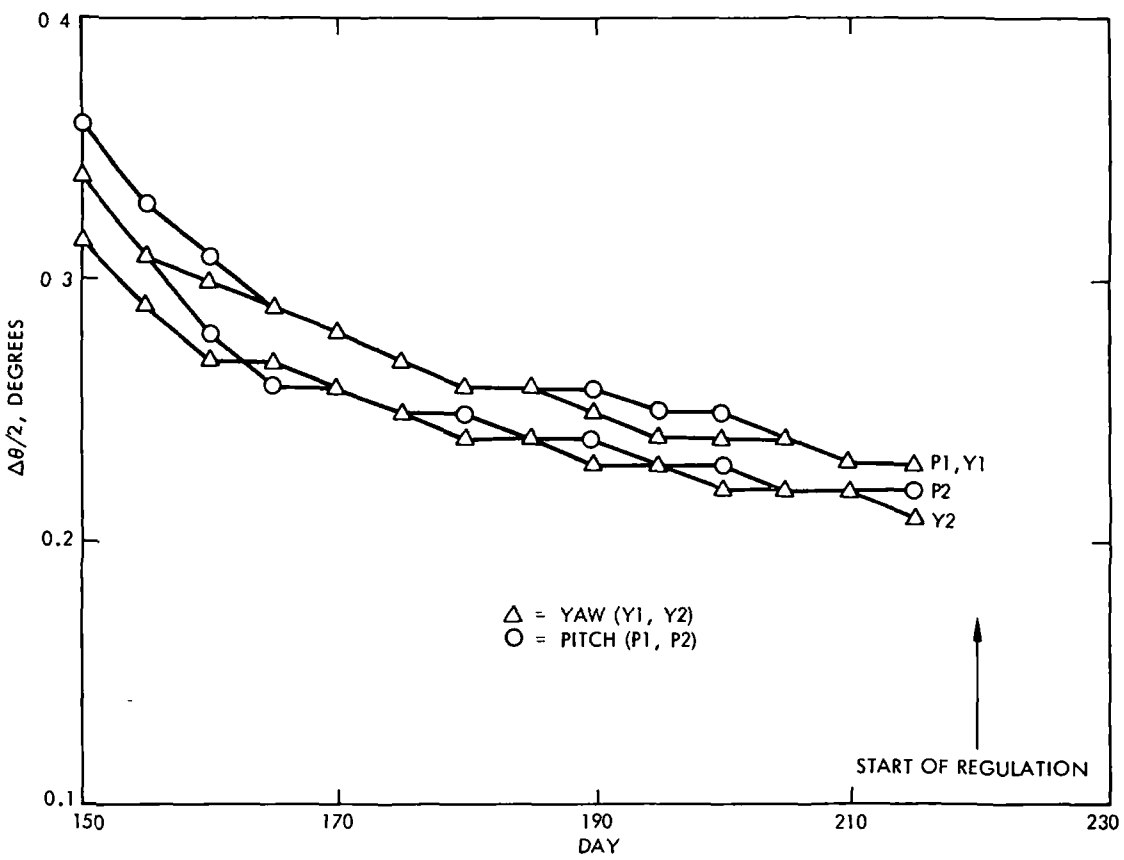

Figure 16. Estimates of Half Deadband Width

5. Acquisition Sensor Resistance in Mars Orbit

A series of tests were run to estimate the effect of Mars illumination on the acquisition sensor resistance. Because of the acquisition sensor geometry, it was determined that the lowest resistance would be achieved if the spacecraft positive roll axis were pointed toward Mars. Although this geometry will not occur in orbit, it is a convenient worse case.

With the positive roll axis pointed toward Mars, the forward looking detectors are half illuminated by the sun, and their resistance is not affected by light from Mars The side looking detectors are illuminated slightly by Mars light when the angular diameter of the planet is sufficiently large. The rear looking detectors are influenced most by Mars light, since they are half illuminated.

The total load resistance of the sun sensors is the parallel combination of the cruise sensors, forward looking acquisition sensors, and the remaining acquisition sensors illuminated only by Mars light.

A planet simulator was used to obtain an estimate of the effect of Mars light on the acquisition sensor resistance. The results for this test are plotted in Figure 17 as a function of simulator intensity. Mars intensity for day 90 of the orbit is given in Figure 18.

The tests indicated there probably would be short periods during each orbit when the sun sensors are out of regulation. This analysis was verified during Mariner 71 orbits: the sun sensors went out of regulation for upwards of thirty minutes near the periapsis of each orbit.

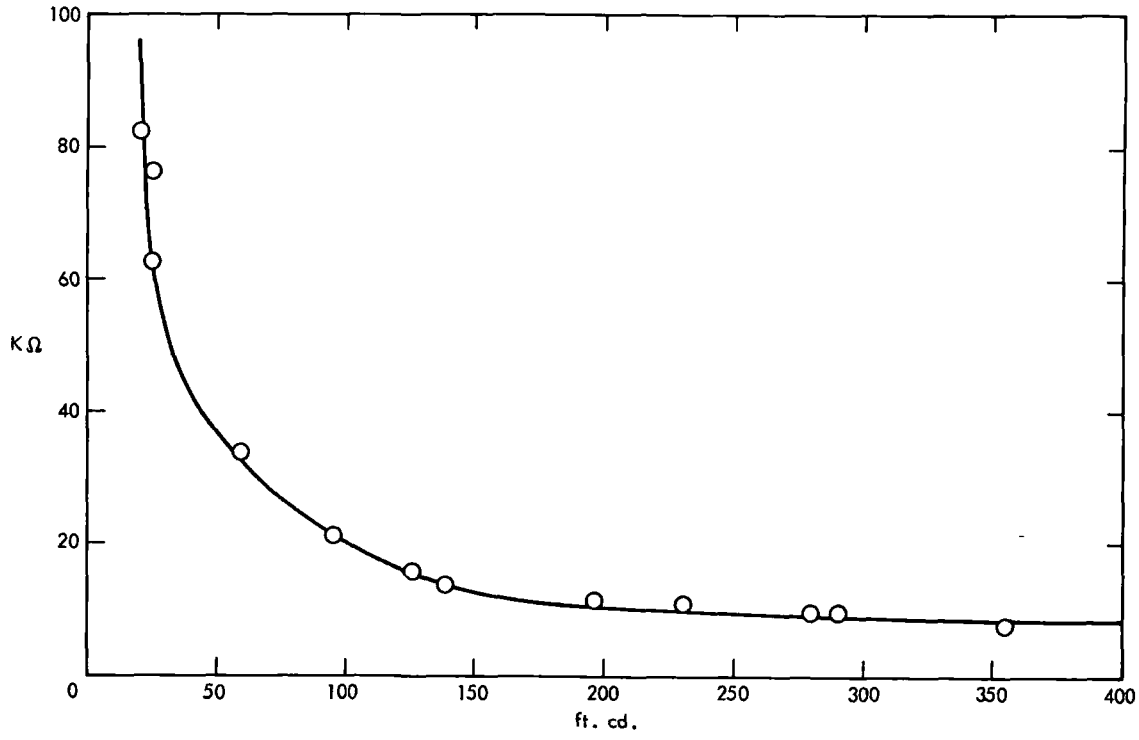

Figure 17. Parallel Resistance of Acquisition Detectors as a Function of Intensity

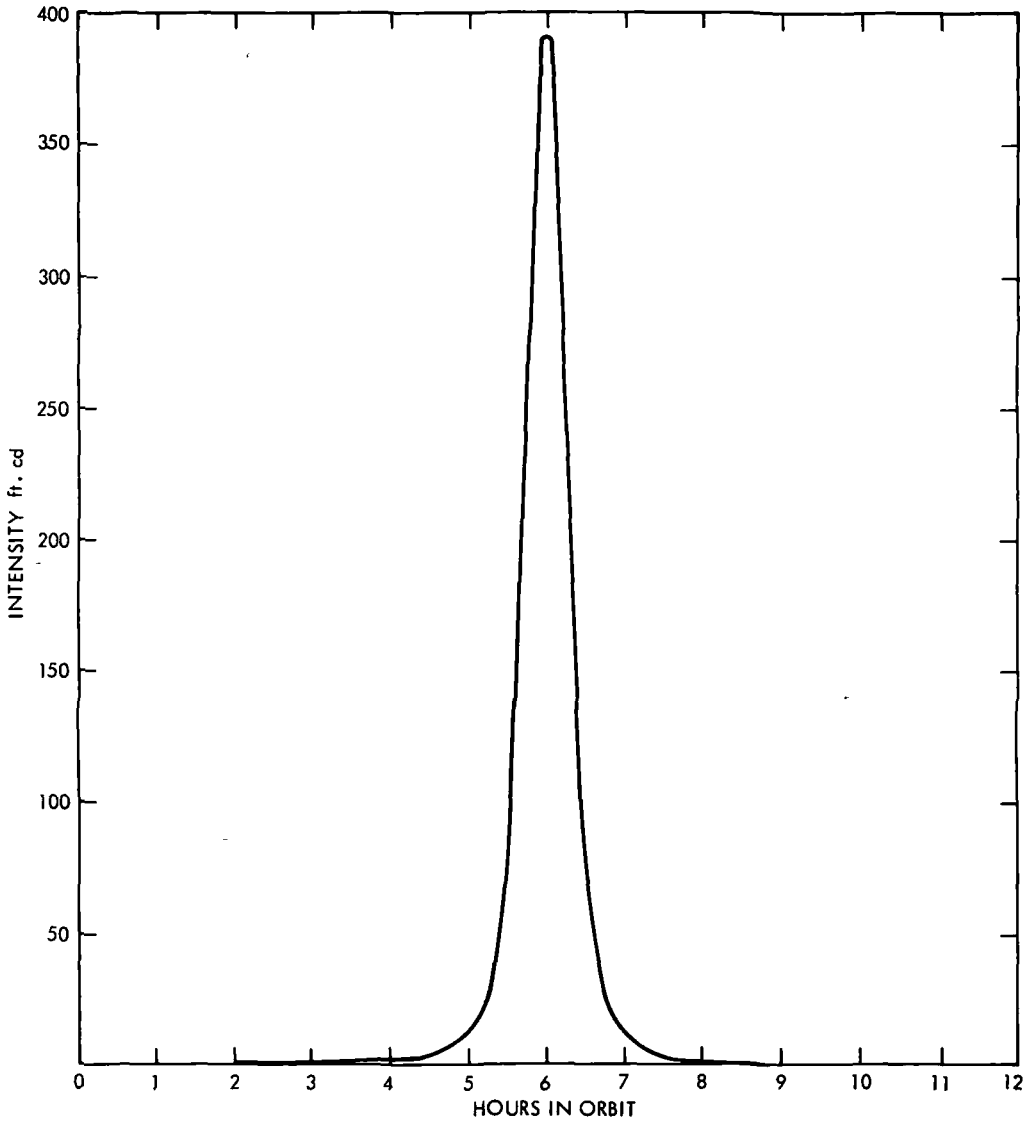

Figure 18. Mars Intensity on Day 90 of Orbit

B. MARINER 71 RCA GAS VALVE LEAKAGE IDENTIFICATION AND EVALUATION

1. The Problem

The Mariner 71 spacecraft utilizes a reaction control assembly (RCA) to provide attitude control torques. The system consists of tanks, plumbing, and solenoid operated valves, and it contains nitrogen gas Because of limitations in the state-of-the-art fabrication and cleaning methods, the RCA can expect to

experience valve leaks. The cause of the leaks is system contamination and/or valve mechanism imperfections Regardless of the cause of a valve leak, the offending valve must be identified, and the magnitude of the leak must be known if corrective action is to be taken.

2. Identifying a Leaking Valve

A leaking valve develops a thrust proportional to the leak rate. This thrust produces a torque on the spacecraft which may be observable in one or more of the spacecraft axes as parabolic curves of spacecraft position error versus time. The RCA gas jet orientation for Mariner 71 is illustrated in Figure 9.

In the pitch and yaw axes, it is not possible from spacecraft data telemetry alone to distinguish between leaking valves of the same polarity. For example, the plot of pitch position telemetry versus time would look exactly the same if valves BXCW or AXCW in Figure 9 were leaking. However, if the leak were allowed to continue for a long period, one of the half-gas systems would indicate a greater consumption than the other, pinpointing the leaking valve.

The axis and polarity of the leakage torque will always isolate a leak to one of two valves in a particular couple. Figure 10 illustrates a spacecraft position error signal when that axis is subject to a positive disturbance torque (assumed from a gas leak) On Mariner 71, the relationship of parabolic orientation to torque polarity is the same in all spacecraft axes.

The process by which a leaking BZCW valve induces a disturbance torque in all three spacecraft axes is illustrated in Figure 19. The roll valves lie in the pitch and yaw plane but their thrust axes makes an angle of 21 degrees with the yaw axis. When a leaking roll valve's thrust is resolved into components parallel to the principal spacecraft axes, and the position of the spacecraft center of mass is known, evaluation of the disturbance torques in all spacecraft axes can be performed readily.

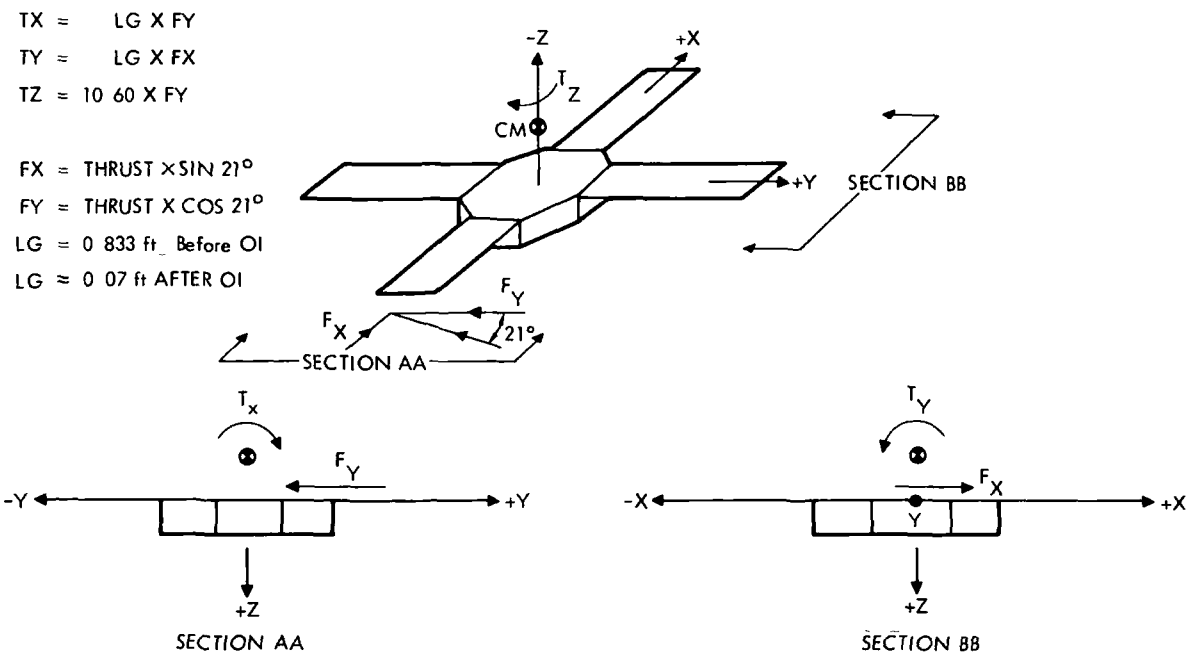

Figure 19. Disturbance Torque Configuration Resulting From a Leaking Roll Valve on the -X Panel

C. EVALUATION OF LEAKAGE TORQUE MAGNITUDE

1. Identification and Correction of Leakage Torque

Given spacecraft position telemetry data, plotted as in Figure 10, the disturbance torque magnitude can be evaluated as follows:

$$Td = 8J \frac{\Delta\theta}{\Delta t^2} \tag{39}$$

where

J = spacecraft inertia in the axis of interest in kg-m^2

$\Delta\theta$ = height of parabolic curve in radians

Δt = the time between gas jet firings

Td = disturbance torque in newtons-m

Families of constant disturbance torque curves are shown in Figure 20. Also shown: the leakage magnitude in the roll axis which would produce the curves, given the observed telemetry values of $\Delta\theta$ and Δt.

Spacecraft telemetry data are sufficiently accurate to identify all gas leaks which exceed design specification. The problem remains to determine a course of action in the event a leak requires corrective measures. In general, corrective action includes cycling the leaking valve at least once, and possibly several times. When the valve is open, seat contamination may be flushed out by the nitrogen flow, allowing the valve to reseat completely.

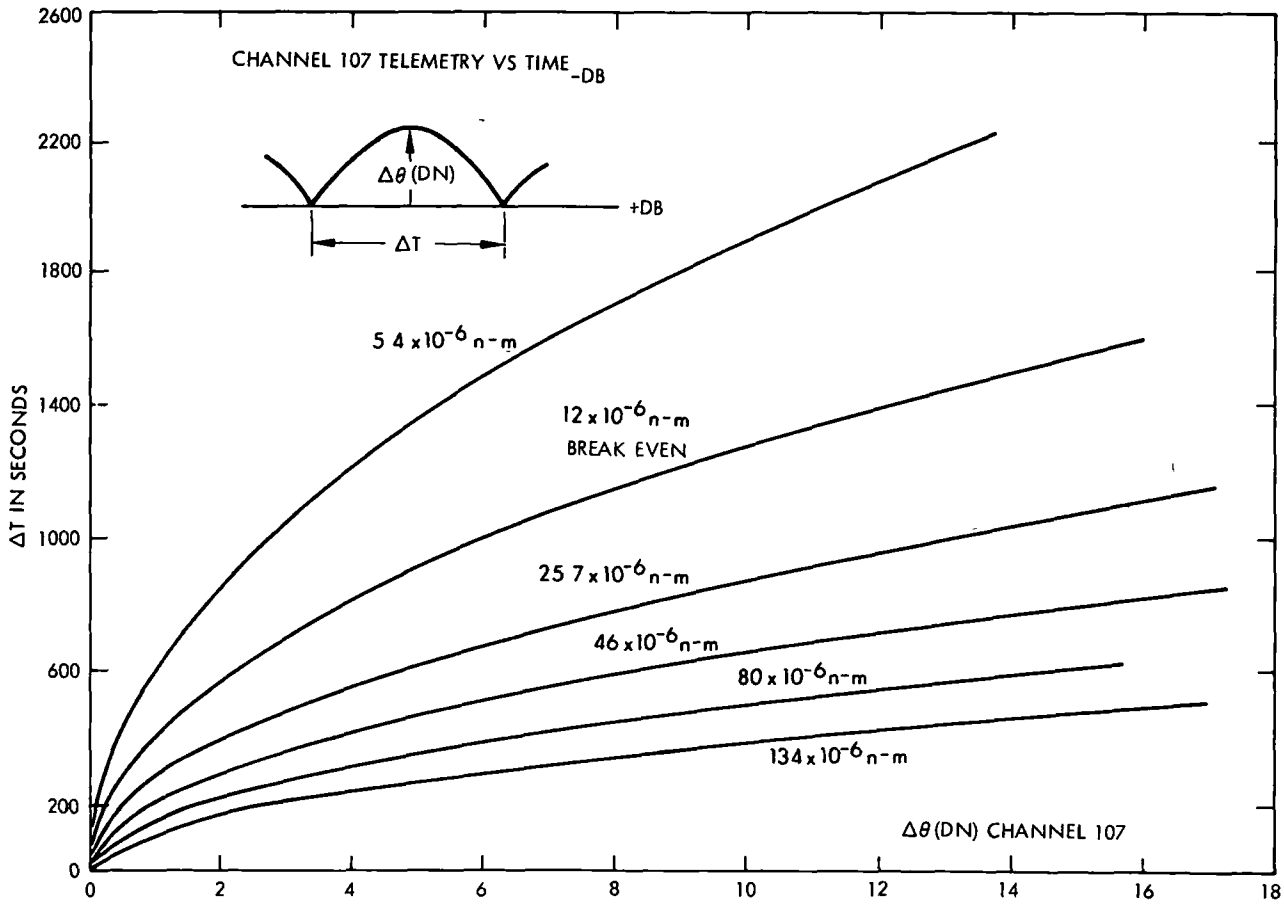

Figure 20. Roll Axis Leakage Torque Magnitude

On Mariner 71, valve cycling will occur when gyros are turned on or off. Gyros can be activated with either ground or computer commands.

The ground command method was used about 100 times during the Mariner 71 orbital cruise period when the spacecraft was monitored on a twenty-four hour basis, and flight computer commands were used in the solar occultation period when around-the-clock spacecraft visibility was not possible.

V. DYNAMIC INTERACTION BETWEEN MARINER 71 BUS AND THE SCAN PLATFORM

The Mariner 71 scan platform is used to support and point the scientific instruments and TV cameras The scan platform has two angular degrees of freedom relative to the spacecraft bus, called the clock and cone angles. The clock axis is parallel to the spacecraft roll axis The cone axis is in a plane defined by the pitch and yaw axes. A typical scan slew is performed at an average slew rate of 4 4 mrad (0 25 degree) per second, the first slew being the clock slew, followed one second later by the cone slew.

The on-board computer issues one command each second to either a clock or cone axis sequencing circuit. The sequencing circuit issues four commands to a stepper motor, causing the motor to rotate 90 degrees with each command. In this manner, the last rotation of the driver stepper motor is executed about one-half second after receipt of the computer command. The stepper motor drives a reference potentiometer which provides the reference signal to the scan actuator drive circuits The stepper motor actuation sequence is described in Figure 21. The illustration includes the scan platform response and the dynamic actuator model used to model stepper motor-gear train-scan platform response characteristics. The spring constant of the actuator mechanism was determined in preflight testing, but the damping coefficient could be only estimated.

The analysis presented below demonstrates that the spacecraft rate induced by a scan slew was up to fifty percent greater than anticipated, and that small variations in the damping coefficient can produce large changes in the quantity of gas used when slewing in the all-axis inertial mode

The Mariner 71 configuration with the cone axis aligned with either the pitch or yaw axis is shown in Figure 22. When all products of angular rates are assumed small, the equations of motion about the axis in question are given as follows:

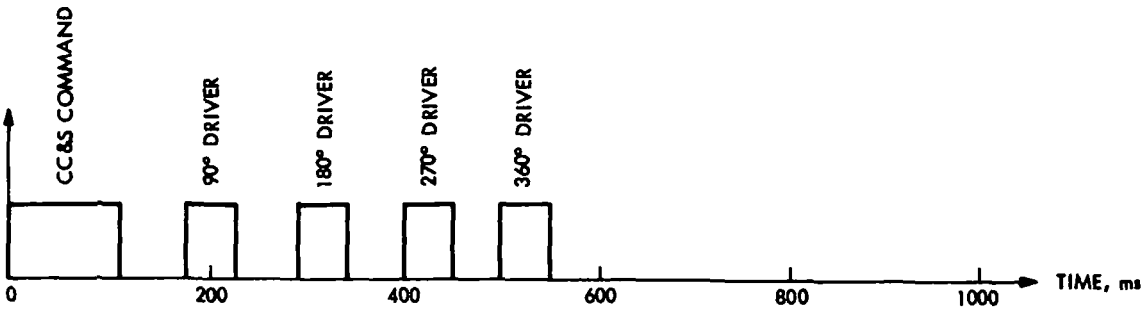

LOGIC SEQUENCE FOR SCAN STEPPER MOTOR COMMANDS

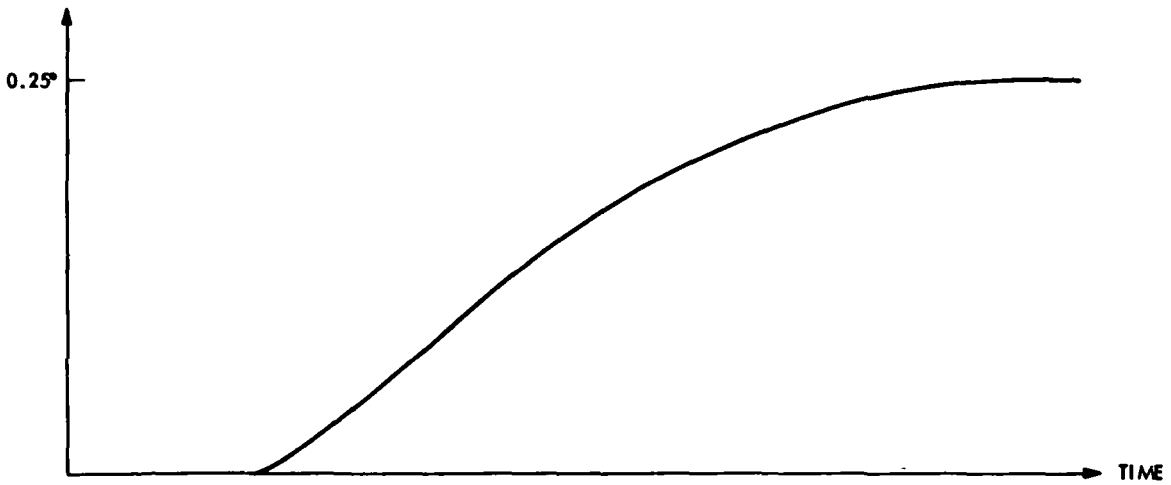

SCAN ACTUATOR DISPLACEMENT

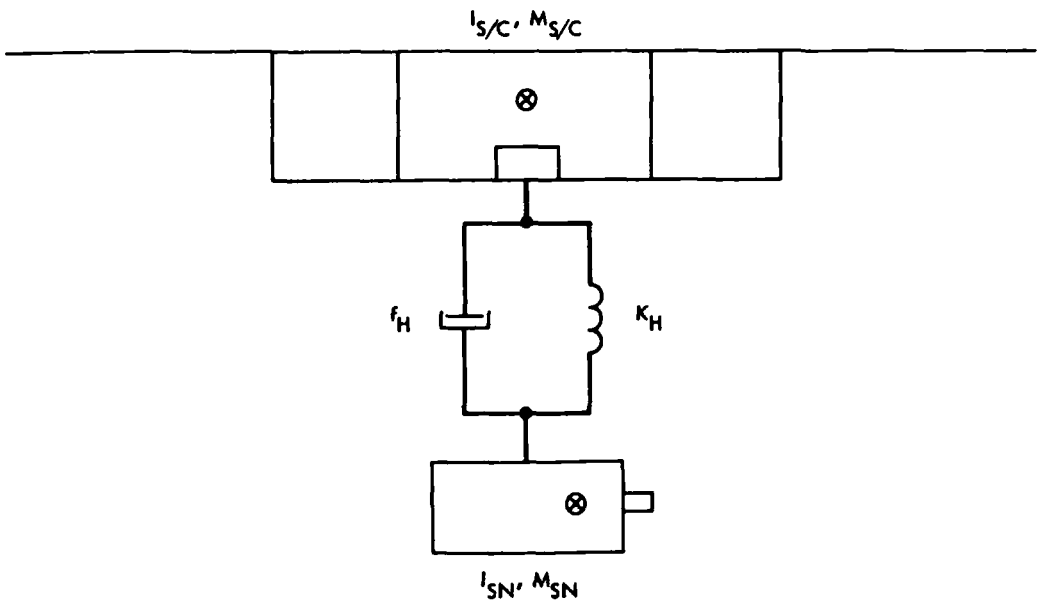

Figure 21. Scan Actuator Module

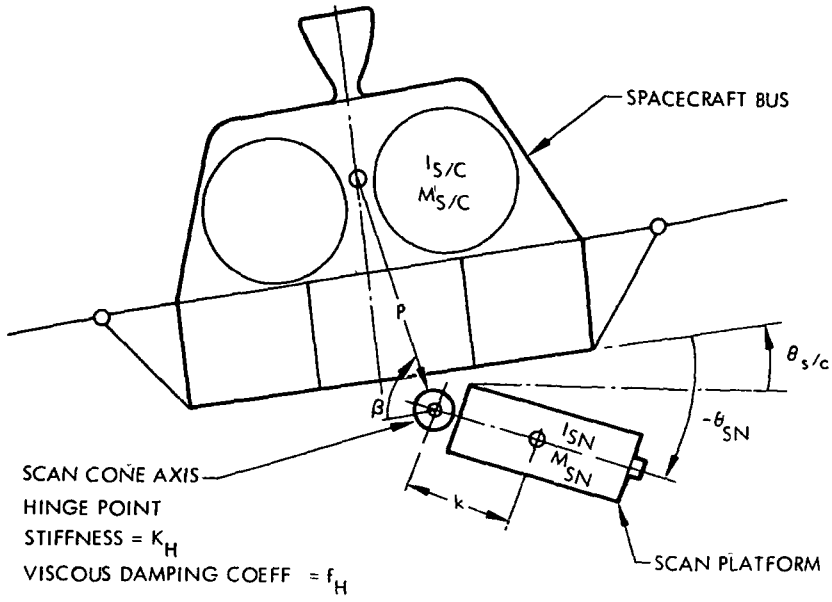

Figure 22. Scan Platform Cone Axis Configuration

$$\left[I_{s/c} + mp^2 + mpk \cos (B + \theta_{sn})\right] \theta_{s/c} + mpk \cos (B + \theta_{sn})\, \theta_{sn}$$

$$- f_H \dot{\theta}_{sn} - k_H(\theta_{sn} - \theta_{snc}) = 0 \qquad (40)$$

$$\left[I_{sn} + mk^2\right]\ddot{\theta}_{sn} + \left[mpk \cos (B + \theta_{sn}) + I_{sn} + mk^2\right]\dot{\theta}_{s/c}$$

$$+ f_H \dot{\theta}_{sn} + k_H(\theta_{sn} - \theta_{snc}) = 0 \qquad (41)$$

where

$I_{s/c}$ = spacecraft bus moment of inertia about the axis parallel to the cone axis and through the bus mass center
325 kg-m^2 (240 slug ft^2)

$m_{s/c}$ = mass of the spacecraft bus
484 5 kg (33.2 slugs)

I_{sn} = scan platform moment of inertia about the axis parallel to the cone axis and through the mass center
2 98 kg-m^2 (2.2 slug ft^2)

m_{sn} = mass of the scan platform
74.4 kg (5.1 slugs)

p = distance from the spacecraft bus mass center to the scan actuator
0 64 m (2 1 ft).

k = distance from the actuator to scan platform mass center
0.3 m (0 98 ft)

$$m = \frac{m_{s/c} * m_{sn}}{m_{s/c} + m_{sn}}$$

k_H = spring constant of the scan actuator
= 4068 joules/radian (3000 ft-lbs/radian)

f_H = equivalent viscous damping coefficient of scan actuator, assumed to be 406.8 joules/radian (300 ft-lb/rad/sec)

$\theta_{s/c}$ = inertial spacecraft displacement

θ_{sn} = scan platform displacement relative to spacecraft bus.

Solving for the ratio of the angular accelerations we find that

$$\frac{\dot{\theta}_{s/c}}{\dot{\theta}_{sn}} = -\frac{I_{sn} + mk^2 + mpk \cos(\beta + \theta_{sn})}{I_{s/c} + I_{sn} + m\left[k^2 + p^2 + 2pk \cos(\beta + \theta_{sn})\right]} \tag{42}$$

For the pitch axis this value is approximately -0.0455. When the initial spacecraft rate and scan slew rate is zero, the ratio above is also the ratio of slew rate to spacecraft rate. Prior to the flight of Mariner 71, the ratio of angular accelerations or angular rates was assumed proportional to the ratio of body inertias at the hinge point. In this case, the ratio becomes 0.016, less than half the actual ratio.

If the stepper motor input to the actuator and gear train is approximated as a step input, the Laplace transform of the equation of motion of the platform model in Figure 21 is:

$$I_{sn}S^2\theta_{sn}(S) + f_H S\theta_{sn}(S) + k_H\left[\theta_{sn}(S) - \theta_{snc}(S)\right] = 0 \tag{43}$$

where

S = Laplace operator

$\theta_{sn}(S)$ = Laplace transform of the scan platform cone axis displacement

$\theta_{snc}(S)$ = Laplace transform of the scan platform commanded position

$$= \frac{0.25 \times 0.01745}{S}$$

Solving equation (43) for the Laplace transform of the scan slewing rate gives:

$$S\theta(S) = \frac{0.0044 * k_H}{I_{sn}S^2 + f_H S + k_H} \tag{44}$$

The inverse Laplace transform of equation (44) gives the following expression for the scan slewing rate

$$\dot{\theta}_{sn}(t) = \frac{C}{B}\left[e^{-\frac{f_H t}{2I_{sn}}} \sin (Bt)\right] \tag{45}$$

$$B = \left(\frac{4k_H I_{sn} - f_H^2}{4I_{sn}^2}\right)^{1/2}$$

$$C = 0.0044 * k_H / I_{sn}$$

To determine the maximum rate, the derivative of equation (45) is set equal to zero. This operation gives the following expression

$$\tan (Bt) = \frac{2BI_{sn}}{f_H} \tag{46}$$

The variable t above is determined to be 48.2×10^{-3} sec. When substituted into equation (45) it yields the maximum cone axis relative slewing rate of 32.6×10^{-3} rad/sec.

When the initial spacecraft and slewing rates are zero, the peak spacecraft rate during a 4 4 mrad (0.25 degree) cone axis slew can be evaluated from equation (42) as follows:

$$\dot{\theta}_{s/c}(\max) = -0.0455 \times 32.6 \times 10^{-3}$$

$$= -1482. \times 10^{-6} \text{ rad/sec} \qquad (47)$$

The pitch and yaw rate deadbands are $\pm 614 \times 10^{-6}$ rad/sec. Consequently, if scan slewing is performed in the all axis inertial mode, the deadband will be violated every 4.4 mrad (0.25 degree) scan cone step and result in excessive attitude control gas consumption

In the roll axis, the following parameter changes are required to evaluate the ratio in equation (42):

$$I_{s/c} = 459\ 6 \text{ kg-m}^2 \ (339 \text{ slug ft}^2)$$

$$I_{sn} = 7\ 32 \text{ kg-m}^2 \ (5\ 4 \text{ slug ft}^2)$$

$$\rho \approx 0.24 \text{ m } (0\ 79 \text{ ft})$$

$$k = 0\ 076 \quad (\ 25)$$

The ratio of roll axis acceleration to the scan clock slewing acceleration is 0.021. The peak slewing rate determined from equation (45) is 31.3×10^{-3} rad/sec, and induces a peak spacecraft rate of 700×10^{-6} rad/sec.

A roll axis phase plane in a two body, three axis simulation of a Mariner 71 clock axis slew is illustrated in Figure 11. The illustration is depicted in the roll inertial mode using the parameters described in this report.

The Mariner 71 roll rate deadbands are $\pm 356 \times 10^{-6}$ rad/sec. Therefore, an induced spacecraft rate greater than 700×10^{-6} rad/sec will cause gas jet firings with each new step. A plot of the roll axis gas consumption during the slewing sequence described above is given in Figure 23. Approximating the consumption as a straight line gives the gas usage rate of 0.02×10^{-3} kg/step (0.046×10^{-3} lbs/step), the consumption rate observed in flight. The same simulation produced an average gas usage rate of about 0.04×10^{3} kg/step (0.081×10^{-3} lbs/step) for $f_H = 132$ kg/rad/sec, and about 0.005×10^{-3} kg/step (0.01×10^{-3} lbs/step) for $f_H = 188$ kg/rad/sec.

The Mariner 71 flight data, confirmed by accurate multibody computer simulations, revealed that the current method of scan platform slewing precludes slewing in the inertial mode if conservation of attitude control gas is required

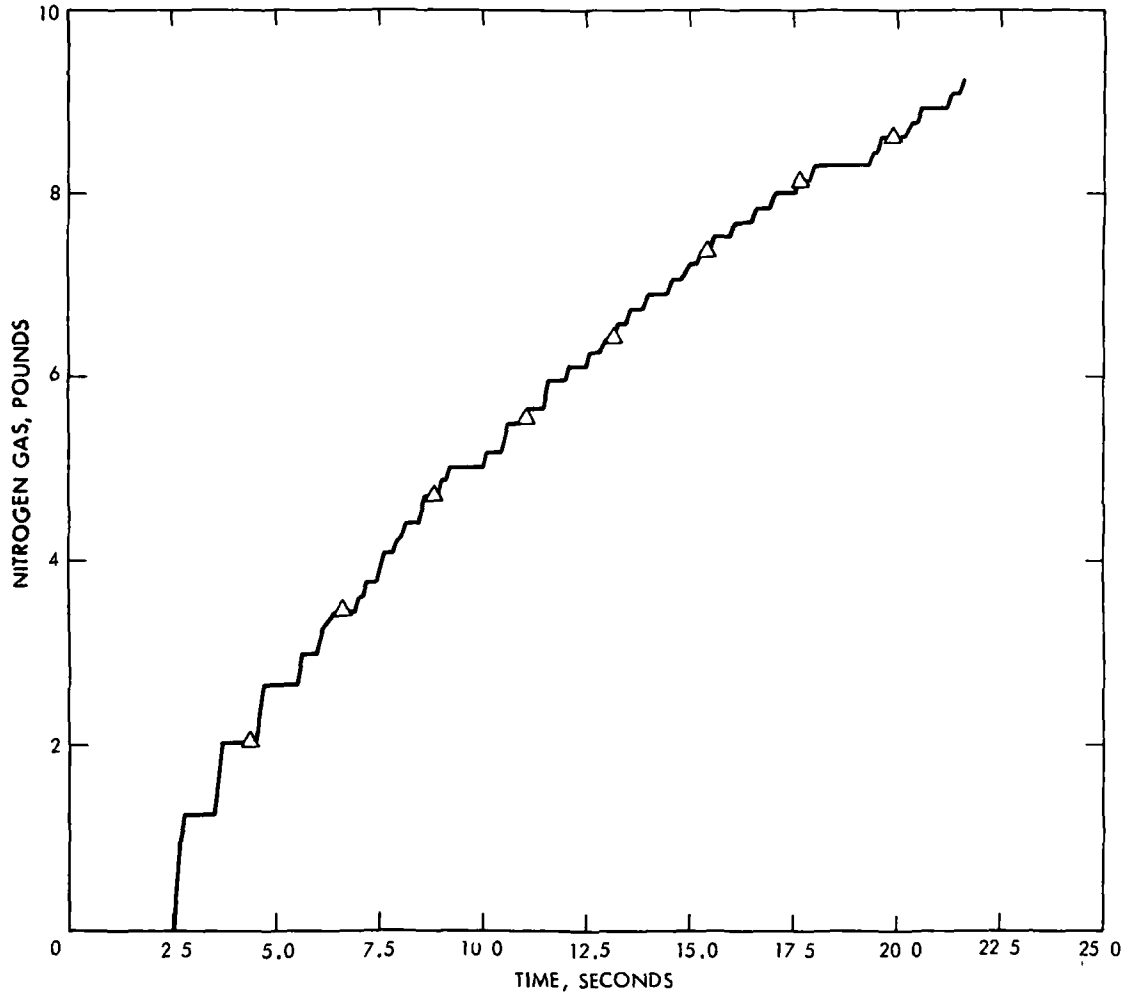

Figure 23. Roll Axis Gas Consumption in Roll Axis Inertial During Scan Slew

VI. ACCOMPLISHMENTS AND CONCLUSIONS

Mariner 71 successfully completed its primary mission and may well complete an extended mission exceeding the most optimistic prelaunch plans. The attitude control subsystem performance was instrumental to the success of every phase of the mission, and consequently must be rated a success

A. ACCOMPLISHMENTS

A large and invaluable store of experience was accumulated during the mission which increased our understanding of the attitude control subsystem and its interaction with other subsystems of the spacecraft.

The Mariner 71 sun sensor interface problem constitutes an example of such experience Design and preflight qualification procedures for the sensor were changed little from that of the Ranger spacecraft. The instrument was simple, reliable, and had performed predictably throughout all previous Mariner missions However, because of a design error incorporated in the Mariner 71 sun sensor interface circuitry, the sensor revealed performance characteristics in the cruise mode which had remained undetected in previous programs This unexpected discovery has resulted in upgrading of sun sensor preflight test procedures and modification of future sensor designs

A parallel example exists in the area of scan platform and attitude control dynamic interaction. As Mariner 71 flight data analysis disclosed that interaction problems existed, analytical and simulation techniques were developed to explain these phenomena. These techniques were then used to influence the design of the Viking and Mariner Jupiter Saturn attitude control subsystems.

B. CONCLUSIONS

Mariner 71 demonstrated that spacecraft design and evaluation does not end with launching of the spacecraft. Actual flight performance is the final and most rigorous test of a subsystem and clearly marks those areas which require further improvement and development.

REFERENCES

1. Crawford, W., Erratic Limit Cycle Behavior on the Mariner IX Spacecraft, IOM 344-104 (an internal document). Jet Propulsion Laboratory, Pasadena, Calif , June 29, 1971.

2. Turk, Will, Ranger Block III Attitude Control System, Technical Report 32-663. Jet Propulsion Laboratory, Pasadena, Calif., Nov. 15, 1964.

3. Fleischer, G. E., Multi-Rigid Body Attitude Dynamics Simulation, Technical Report 32-1516. Jet Propulsion Laboratory, Pasadena, Calif., Feb. 15, 1971.

4. Edmunds, R. S., Recovery of Mariner IX from its Anomalous Operating Mode, EM 344-361 (an internal document). Jet Propulsion Laboratory, Pasadena, Calif., Oct. 1971.

5. Edmunds, R. S., Investigation of the Mariner IX Cold Gas System and Associated Electronics, EM 344-353 (an internal document). Jet Propulsion Laboratory, Pasadena, Calif., July 26, 1971.

NASA — JPL — Coml , L A , Calif

TECHNICAL REPORT STANDARD TITLE PAGE

1. Report No. 33-600	2. Government Accession No.	3. Recipient's Catalog No.
4. Title and Subtitle MARINER MARS 1971 ATTITUDE CONTROL SUBSYSTEM FLIGHT PERFORMANCE		5. Report Date March 15, 1973 6. Performing Organization Code
7. Author(s) L. Schumacher		8. Performing Organization Report No.
9. Performing Organization Name and Address JET PROPULSION LABORATORY California Institute of Technology 4800 Oak Grove Drive Pasadena, California 91103		10. Work Unit No. 11. Contract or Grant No. NAS 7-100 13. Type of Report and Period Covered Technical Memorandum
12. Sponsoring Agency Name and Address NATIONAL AERONAUTICS AND SPACE ADMINISTRATION Washington, D.C. 20546		14. Sponsoring Agency Code

15. Supplementary Notes

16. Abstract

The Mariner Mars 1971 is the fifth generation in an evolutionary spacecraft design with the next design iteration (Viking) to be launched in 1975. Based on knowledge acquired from the successes and limitations of its predecessors, each succeeding generation of spacecraft has been improved and expanded in capability.

This report describes the flight performance of the Mariner 71 Attitude Control Subsystem. Each phase of the mission is delineated and the attitude control subsystem performance is evaluated within the observed operational environment. Performance anomalies are introduced and discussed briefly within the context of general performance. More serious problems, such as the sun sensor interface incompatability, gas valve leaks, and scan platform dynamic coupling effects are given detailed analytical considerations.

It is concluded that the Mariner 71 attitude control subsystem flight performance was satisfactory. The flight experience has increased our understanding of the attitude control process and thereby resulted in improved subsystem designs for future spacecraft.

17. Key Words (Selected by Author(s))	18. Distribution Statement
Control and Guidance Mariner Mars 1971 Project Telemetry and Command	Unclassified -- Unlimited

19. Security Classif. (of this report)	20. Security Classif. (of this page)	21. No. of Pages	22. Price
Unclassified	Unclassified	61	